CONTACT MECHANICS OF GRADED MATERIALS WITH TWO-DIMENSIONAL MATERIAL PROPERTY VARIATIONS

A THESIS SUBMITTED TO
THE GRADUATE SCHOOL OF NATURAL AND APPLIED SCIENCES
OF
MIDDLE EAST TECHNICAL UNIVERSITY

BY

KEMAL GÖKAY

IN PARTIAL FULFILLMENT OF THE REQUIREMENTS
FOR
THE DEGREE OF MASTER OF SCIENCE
IN
MECHANICAL ENGINEERING

SEPTEMBER 2005

Approval of the Graduate School of Natural and Applied Sciences

Prof. Dr. Canan ÖZGEN
Director

I certify that this thesis satisfies all the requirements as a thesis for the degree of Master of Science

Prof. Dr. S. Kemal İDER
Head of Department

This is to certify that we have read this thesis and that in our opinion it is fully adequate, in scope and quality, as a thesis for the degree of Master of Science

Asst. Prof. Dr. Serkan DAĞ
Supervisor

Examining Committee Members

Prof. Dr. Orhan YILDIRIM (METU, ME) _____

Asst. Prof. Dr. Serkan DAĞ (METU, ME) _____

Prof. Dr. Bülent DOYUM (METU, ME) _____

Assoc. Prof. Dr. Suat KADIOĞLU (METU, ME) _____

Asst. Prof. Dr. Bora YILDIRIM (HÜ, ME) _____

I hereby declare that all information in this document has been obtained and presented in accordance with academic rules and ethical conduct. I also declare that, as required by these rules and conduct, I have fully cited and referenced all material and results that are not original to this work.

Name, Last name: Kemal GÖKAY

Signature :

ABSTRACT

CONTACT MECHANICS OF GRADED MATERIALS WITH TWO-DIMENSIONAL MATERIAL PROPERTY VARIATIONS

Gökay, Kemal

M.S., Department of Mechanical Engineering

Supervisor: Asst. Prof. Dr. Serkan Dağ

September 2005, 62 pages

Ceramic layers used as protective coatings in tribological applications are known to be prone to cracking and debonding due to their brittle nature. Recent experiments with functionally graded ceramics however show that these material systems are particularly useful in enhancing the resistance of a surface to tribological damage. This improved behavior is attributed to the influence of the material property gradation on the stress distribution that develops at the contacting surfaces. The main interest in the present study is in the contact mechanics of a functionally graded surface with a two – dimensional spatial variation in the modulus of elasticity. Poisson's ratio is assumed to be constant due to its insignificant effect on the contact stress distribution [30]. In the formulation of the problem it is assumed that the functionally graded surface is in frictional sliding contact with a rigid flat stamp. Using elasticity theory and semi-infinite plane approximation for the graded medium, the problem is reduced to a singular integral equation of the second kind. Integral equation is solved numerically by expanding the unknown contact stress distribution into a series of Jacobi polynomials and using suitable collocation points. The developed method is validated by providing comparisons to a closed form solution derived for homogeneous materials. Main numerical results consist of the effects of the material nonhomogeneity parameters, coefficient of friction and stamp size and location on the contact stress distribution.

Keywords: Contact Mechanics, Functionally Graded Materials, Sliding Contact, Singular Integral Equations

ÖZ

İKİ BOYUTLU MALZEME ÖZELLİĞİ DEĞİŞİMİ OLAN
DERECELENDİRİLMİŞ MALZEMELERİN TEMAS MEKANİĞİ

Gökay, Kemal
Yüksek Lisans, Makina Mühendisliği Bölümü
Tez Yöneticisi: Y. Doç. Dr. Serkan Dağ

Eylül 2005, 62 sayfa

Tribolojik uygulamalarda koruma kaplaması olarak kullanılan seramik tabakalar doğal kırılganlıklarından dolayı çatlamaya ve ayrılmaya eğilimlidir. Fonksiyonel derecelendirilmiş seramikler ile ilgili son deneyler bu malzeme sistemlerinin özellikle yüzeyin tribolojik hasarlara olan direncini kuvvetlendirmede yararlı olduğunu göstermektedir. Bu geliştirilmiş davranış temas yüzeylerinde gelişen gerilme dağılımındaki malzeme özelliği değişiminin etkisine bağlanmıştır. Bu çalışmanın ana ilgi alanı elastisite modülündeki iki boyutlu düzlemsel değişimli fonksiyonel derecelendirilmiş yüzeyin temas mekaniğidir. Temas gerilme dağılımındaki önemsiz etkileri sebebiyle Poisson oranın sabit olduğu varsayılmıştır. Problemin formülasyonunda fonksiyonel derecelendirilmiş yüzeyin rijit düz zımba ile kayma temasında olduğu varsayılmıştır. Problem ikinci tür tekil integral denklemine elastisite teorisi ve derecelendirilmiş ortam için yarı sonsuz düzlem yaklaşımı kullanarak indirgenmiştir. İntegral denklemi sayısal olarak temas gerilme dağılım bilinmeyenlerini Jacobi polinomları serilerine açılarak ve uygun sıralama noktaları kullanarak çözülmüştür. Geliştirmiş metodun doğruluğu homojen malzeme için türetilmiş kapalı biçim çözümüyle karşılaştırılarak sınanmıştır. Ana sayısal sonuçlar derecelendirme parametreleri, sürtünme katsayısı ve temas gerilme dağılımı üzerindeki zımba boyutu ve konumu etkilerini içermektedir.

Anahtar kelimeler: Temas Mekaniği, Fonksiyonel Olarak Derecelendirilmiş Malzemeler, Kaymalı Temas, Tekil İntegral Denklemleri

To my Parents

ACKNOWLEDGEMENTS

I would like to express my deep gratitude to my supervisor Asst. Prof. Dr. Serkan DAĞ for his continuous supervision, guidance and support during my study, sharing his experience and giving me the chance of meeting contact mechanics.

I would also like to thank to my parents Mr. Dünar GÖKAY and Mrs. Zülal GÖKAY, my brother Mr. Alp GÖKAY, my best friends Mr. Alper SOYLU and Mr. Erdem DÜLGER and my colleagues for supporting me.

TABLE OF CONTENTS

LIST OF FIGURES

FIGURES

LIST OF SYMBOLS

μ	: Shear modulus
γ, β	: Nonhomogeneity parameters
v	: Poisson's ratio
κ	: *(3-4v)* for plane strain, *(3-v)/(1+v)* for plane stress
P	: Normal force
η	: Coefficient of friction
a ,b	: End points of the contact area
u ,v	: Displacement components in x- and y- directions
σ_{ij}	: Stress components ($i,j = x,y$)
s_j	: Roots of the characteristic equations (j = 1,2,3,4)
ρ	: Fourier Transform variable
A_{1j}	: Integration cut-off points (i = 1, 2, 3, 4)
$(\gamma+\beta)^*,(\gamma+\beta)^{**}$	: Normalized nonhomonegeity parameters
$P_n^{(\beta_1,\beta_2)}$	: Jacobi polynomials
β_1, β_2	: Strengths of the singularity
N	: Number of collocation points

CHAPTER 1

INTRODUCTION

1.1 Functionally Graded Materials (FGMs)

The needs on materials increase as the technology improves. Materials have to withstand more severe conditions. In order to overcome this problem scientists firstly developed traditional composite materials. But this homogeneous materials' specification seems to be restricted. The internal stresses caused by the elastic and thermal properties mismatch at an interface between two different materials can mitigate the successful implementation of such traditional composites. To solve this problem, scientists secondly developed functionally graded materials (FGMs) to satisfy the needs for properties that are unavailable in any single material and for graded properties to offset the adverse effects of discontinuities [1].

FGMs offer great promise in applications where the operating conditions are severe. For example, wear-resistant linings for handling large heavy abrasive ore particles, rocket heat shields, heat exchanger tubes, thermoelectric generators, heat-engine components, plasma facings for fusion reactors, and electrically insulating metal/ceramic joints ([2]-[5]). They are also ideal for minimizing thermo mechanical mismatch in metal-ceramic bonding. The bonded structure develops very high residual and thermal stresses because of the relatively high mismatch in thermal expansion coefficients, so the composite medium becomes very susceptible to cracking, debonding and spallation [6].

In order to minimize these incompatibilities and so in order to decrease thermal stresses FGMs are used. In these materials the graded structure protect the metal against to corrosion, oxidation or wear resistance, beside this the graded structure minimize brittleness of homogeneous ceramic coatings and also surface cracks. An

excellent review of FGM subject can be scrutinized in [7]. FGMs have given for example, the possibility to combine the best properties of metals and ceramics- the toughness, electrical conductivity and machinability of metals, and the low density, high strength, high stiffness and temperature resistance of ceramics, taking away the brittleness of ceramics and making strong metals lighter and stiffer.

FGMs were first proposed in around 1984-85 while a researcher was studying aerospace and advanced materials. The body of space plane has to be exposed to very high temperature environment (about 1700 °C), therefore, is required to resist a severe condition generated from a temperature difference (about 1000 °C difference) between inside and outside of the space plane. There was no uniform material capable of enduring to such condition before. Therefore, the researchers devised a concept of FGM that was to fabricate a material by gradually changing (grading) the composition and to improve both thermal resistance and mechanical properties. They considered that fabricating FGM with ceramic would be able to expose to high temperature environment at the surface.

In 1987, FGM research was selected for a big project supported by the Ministry of Education and Science in Japan. From 1987 to 1991, a research project called the "Research on the Generic Technology of FGM Development for Thermal Stress Relaxation" was conducted, and many researchers from universities, national research institutes and corporations took a part of it. In the project, they intensively discussed on material development methods, and established a collaboration system consisting of material design, production and evaluation. The research resulted in generation of the thermal stress relaxing material [8]. There are a lot of fields that FGMs are used such as the thermal barrier coatings (TBCs). TBCs are used as thermal insulators in high temperature chambers, furnace liners, gas turbines, micro-electronics, combustors and vane and blade platforms of aircraft engines [9]. FGMs also proved to be highly effective when utilized as protective coatings against

tribological damage (e.g., wear and brittle fracture due to sliding contact) ([10]-[11]). Many fields of applications are underway such as abradable seals used in stationary gas turbines and load transfer components which are typically gears, cams and bearings.

1.2 Previous Work on Contact Mechanics of Nonhomogenous Materials

Scientists have been working on contact mechanics over a century. The main field in contact mechanics is the analysis of the stress and displacement fields due to contact loadings. The highest stress takes place generally in the contact region that may cause failures through any of the mechanisms of fatigue, spallation, wear and cracks. The first study in contact mechanics was conducted by Hertz [12]. His study has paved way for the solution of the frictionless contact problem of two elastic bodies of ellipsoidal profile. The review of this study can be found in the article of Barber and Ciavarella [13].

Nonhomogeneity can be found in the nature, hence there are a lot of studies for the contact mechanics problems for nonhomogenous materials. Gibson [14] and Calladine and Greenwood [15] considered the problem of point and line loading acting on the bounding surface of an elastic incompressible half plane with a linear variation in elastic modulus. Brown and Gibson [16] made the assumption of incompressibility and constant Poisson's ratio between zero and one-half, Awojobi and Gibson [17] showed the results for axisymmetric half-space, and Gibson and Sills [18] continued to work on nonhomogeneous materials for orthotropic elastic semi-infinite medium. Kassir [19] studied the indentation of an elastic half space by stamps with arbitrary profile. In his study Kassir considered a frictionless contact problem. The shear modulus is assumed to have a power low type of variation in the depth direction. Bakırtaş [20] examined frictionless planar stamp problems. The elastic modulus was assumed to vary exponentially in the depth direction. Kassir and Bakırtaş assumed constant Poisson's ratios in their studies. Fabrikant and Sankar [21] examined axisymmetric contact problems for nonhomogeneous half-space

whose elastic modulus is a power function of the depth coordinate. Selvadurai and coworkers ([22]-[24]) also have some studies on axisymmetric contact problems for nonhomogeneous half-space with elastic non-homogeneity.

Due to the promising properties of FGMs many scientists have tried to characterize the behavior of FGMs and discover their usage areas. Suresh and coworkers [25]

worked on polycrystalline alumina infiltrated with aluminosilicate glass to prove that gradients in elastic modulus at a surface may enhance the resistance against cracking due to the sliding contact. In this study they used a functionally graded alumina-aluminosilicate glass FGM using infiltration method. At high temperatures aluminosilicate glass penetrates into grain boundaries of alumina. The elastic modulus is increased continuously by 50% from the contact surface to a depth beneath the surface. The principal tensile stresses introduced by sliding contact are reduced by the gradation in elastic modulus and finally they presented experimental and computational results that show the glass-infiltrated alumina is more resistant to a contact damage than either monolithic alumina or glass or alumina glass composite. In this study it was seen that the resistance of a surface to frictional sliding contact was increased. Hence FGM can be used as a protective coating against wear resistance and cracking. Giannakopoulos and Suresh [26] worked on the indentation of a half-space by a point force. The same scientists [27] studied the results of analytical and computational stress and displacement field in a graded elastic half space due to indentation by a rigid axisymmetric indentor. Giannakopoulos reviewed the analytical, computational and experimental results on the spherical indentation of a graded elastic half space. Giannakopoulos and Pallot [28] considered a two dimensional sliding contact problem for an elastic graded half plane assuming a power law type of variation for the elastic modulus. The disadvantage of this study is that the elastic modulus becomes zero at the contact surface which is unrealistic. Güler [29] studied the sliding contact problem for FGM coatings loaded by a stamp with an arbitrary profile. He considered an exponential variation for the elastic modulus. The sliding contact problem for rigid stamps and for two contacting FGM coatings were reduced to singular integral equations which was solved by using collocation method.

Failure in tribological applications results from high stresses in the contact surfaces and occurs in the form of cracking in brittle materials and plastic deformation in ductile materials. This failure is generally the initiation and propagation of surface cracks due to oscillatory contact loading at the contact surfaces. Dağ [30] solved this problem by examining the coupled fracture and contact mechanics problem. In his study, he considered an elastic half plane FGM medium with an exponential type of

variation of the elastic modulus loaded by a stamp with arbitrary profile. Dağ and Erdoğan [32] examined the initiation and subcritical growth of surface cracks in FGMs. The coupled crack/contact problem for a nonhomogeneous half-plane is considered in this study. The reader may refer to Dağ and Erdoğan [31] and [32] for more details about the results found.

Özatağ [33] examined the effects of material nonhomogeneity and friction on contact stresses and singularities at end of the contact region for materials with lateral nonhomogeneity. He developed a technique to study the effect of the lateral nonhomogenities on the contact stress distribution for a graded surface. As a result he found that the contact stress distribution is distorted to take the shape of the shear modulus variation. These studies and theoretical analysis show that FGMs is perfectly suitable for applications that require wear or cracking resistance.

1.3 Motivation and Scope of the Study

The studies that are mentioned above are about the effects of depth direction nonhomogenities or lateral direction nonhomogenities. In this study a method is developed to examine the contact mechanics problem for a nonhomogeneous elastic medium by assuming that there is a material nonhomogeneity both in lateral direction and thickness directions. The graded surface is assumed to be isotropic, so shear modulus variation can be expressed as $\mu(x,y)=\mu_o e^{\beta x+\gamma y}$. In this equation μ_o is the shear modulus at x=0 and y=0, β and γ are the nonhomogeneity constants which have a unit of 1/length and can be used for curve-fit purposes. Poisson's ratio is also assumed to have a constant value. The main unknown is the contact stress distribution at the contact surface.

The problem considered is a mixed boundary value problem. In such studies the governing equations is reduced to a singular integral equation (SIE). The SIE can be solved numerically by using orthogonal polynomials. The technique of the solution of the SIE applied to the mixed boundary value problems in mechanics can be found in Erdoğan's [34] study.

In Chapter 2, we formulated the problem using Fourier Transformations and reduce the problem to a SIE. In Chapter 3 the problem is solved numerically using a collocation method. A computer program is developed by using Visual Fortran language to develop numerical solution. In Chapter 4 numerical results and discussions are presented.

CHAPTER 2

FORMULATION

2.1 Derivation of the Singular Integral Equation for the Contact Mechanics Problem

The general description of the sliding contact problem is shown in Figure 1.

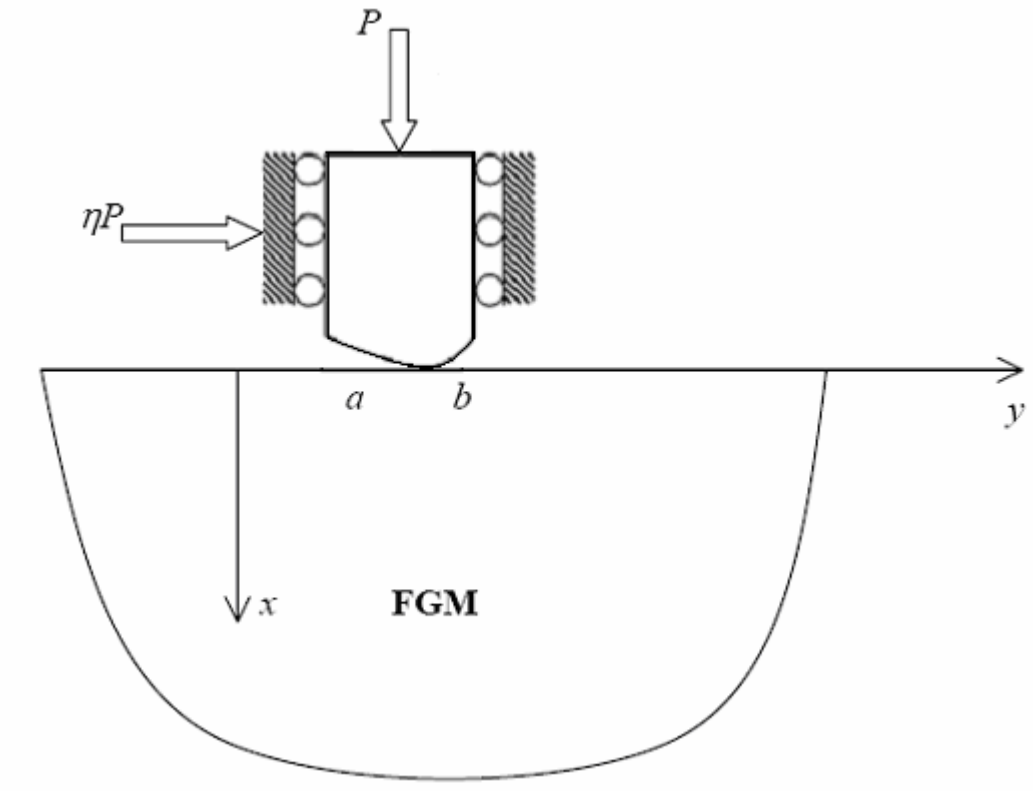

Figure 1: The general description of the contact problem in FGM

Top surface of the half plane is in sliding contact with a rigid stamp of arbitrary profile. The forces are transmitted across the contact surface to the medium with the

normal force P and tangential force ηP where η is the coefficient of friction and contact area extends from a to b.

In this section of the study the problem will be formulated and reduced to a singular integral equation. The effects of material non-homogeneity, friction on contact stresses and singularities at the ends of the contact region will be examined by solving the problem. The shear modulus is defined by;

$\mu(x,y)=\mu_o e^{\beta x+\gamma y}$, κ=constant (1a,b)

In equation (1) the symbols β and γ define the non-homogeneity parameters. Here

- κ=3-4ν for plain strain,
- κ= (3-ν) / (1+ ν) for plane stress.

ν is the Poisson's ratio. Dağ [30] found that the contact stresses in FGM are not affected by ν. So, it assumed that ν will be constant.

By neglecting the body forces, the equations of equilibrium can be obtained as:

$$\frac{\partial \sigma_{yy}}{\partial y}+\frac{\partial \sigma_{xy}}{\partial x}=0 \tag{2a}$$

$$\frac{\partial \sigma_{xx}}{\partial x}+\frac{\partial \sigma_{xy}}{\partial y}=0 \tag{2b}$$

Assuming small deformations and plane stress or plain strain for the isotropic linear elastic medium considered, Hooke's Law is written as follows:

$$\sigma_{xx}(x,y)=\frac{\mu(x,y)}{\kappa-1}\left((\kappa+1)\frac{\partial u}{\partial x}+(3-\kappa)\frac{\partial v}{\partial y}\right) \tag{3a}$$

$$\sigma_{yy}(x,y)=\frac{\mu(x,y)}{\kappa-1}\left((\kappa+1)\frac{\partial v}{\partial y}+(3-\kappa)\frac{\partial u}{\partial x}\right) \tag{3b}$$

$$\sigma_{xy}(x,y)=\mu(x,y)\left(\frac{\partial u}{\partial y}+\frac{\partial v}{\partial x}\right) \tag{3c}$$

Substituting equations (3) in (2); the governing equations for the displacements can be written as,

$$(\kappa+1)\frac{\partial^2 u}{\partial x^2}+(\kappa-1)\frac{\partial^2 u}{\partial y^2}+2\frac{\partial^2 v}{\partial x\partial y}+\beta(\kappa+1)\frac{\partial u}{\partial x}+\gamma(\kappa-1)\left(\frac{\partial u}{\partial y}+\frac{\partial v}{\partial x}\right)+\beta(3-\kappa)\frac{\partial v}{\partial y}=0 \tag{4a}$$

$$(\kappa-1)\frac{\partial^2 v}{\partial x^2}+(\kappa+1)\frac{\partial^2 v}{\partial y^2}+2\frac{\partial^2 u}{\partial x\partial y}+\gamma(3-\kappa)\frac{\partial u}{\partial x}+\beta(\kappa-1)\left(\frac{\partial u}{\partial y}+\frac{\partial v}{\partial x}\right)+\gamma(\kappa+1)\frac{\partial v}{\partial y}=0 \tag{4b}$$

If we examine the Figure 1, the boundary conditions given below have to be satisfied for the solution of the problem;

- Since no load is applied on the outer surface of the contact area,

$$\sigma_{xx}(0,y)=0 \quad , \qquad \sigma_{xy}(0,y)=0 \quad , \qquad -\infty < y < a \, , b < y < \infty \tag{5a,b}$$

- By using the Coulomb's law for frictional contact problems, the shear stresses in the contact area are;

$$\sigma_{xy}(0,y)=\eta \;\; f(y) \quad , \qquad \sigma_{xx}(0,y)=f(y) \quad , \qquad a < y < b \tag{6a,b}$$

- The equilibrium equation is given by

$$\int_a^b \sigma_{xx}(0,y)=-P \tag{7}$$

Considering the Fourier transform in the *y*-direction, the solutions $u(x,y)$ and $v(x,y)$ can be expressed as

$$u(x,y)=\frac{1}{2\pi}\int_{-\infty}^{+\infty}U(x,\rho)\exp(i\rho\, y)\,d\rho \tag{8a}$$

$$v(x,y)=\frac{1}{2\pi}\int_{-\infty}^{+\infty}V(x,\rho)\exp(i\rho\, y)\,d\rho \tag{8b}$$

where $i=\sqrt{-1}$ and $U(x,\rho)$ and $V(x,\rho)$ are the Fourier transform of respectively $u(x,y)$ and $v(x,y)$. The aim of using the Fourier transform is to convert the partial differential equations into ordinary differential equations. Substituting (8a, 8b) into (4a, 4b),

$$\begin{aligned}&(\kappa+1)\frac{d^2U}{dx^2}+2i\rho\frac{dV}{dx}+(\kappa-1)(-\rho^2)U+\beta(\kappa+1)\frac{dU}{dx}+\gamma(\kappa-1)(i\rho)U\\&+\gamma(\kappa-1)\frac{\partial V}{\partial x}+(i\rho)\beta(3-\kappa)V=0\end{aligned} \tag{9a}$$

$$\begin{aligned}&(\kappa-1)\frac{d^2V}{dx^2}+2i\rho\frac{dU}{dx}+(\kappa+1)(-\rho^2)V+(3-\kappa)\gamma\frac{dU}{dx}+\beta(\kappa-1)\frac{\partial V}{\partial x}\\&+\beta(\kappa-1)(i\rho)U+\gamma(\kappa+1)(i\rho)V=0\end{aligned} \tag{9b}$$

Above equations are a set of second order ordinary differential equations which can be written in a matrix form;

$$\begin{bmatrix}a & b\\ c & d\end{bmatrix}\begin{bmatrix}U\\ V\end{bmatrix}=\begin{bmatrix}0\\ 0\end{bmatrix} \tag{10}$$

where a, b, c and d are operators and are given as follows

$$a=s^2(\kappa+1)+\beta(\kappa+1)s+(\kappa-1)(-\rho^2+\gamma i\rho) \tag{11a}$$

$$b=s[2i\rho+\gamma(\kappa-1)]+\beta i\rho(3-\kappa) \tag{11b}$$

$$c=s[2i\rho+\gamma(3-\kappa)]+\beta i\rho(\kappa-1) \tag{11c}$$

$$d=s^2(\kappa-1)+\beta(\kappa-1)s+(\kappa+1)(-\rho^2+\gamma i\rho) \tag{11d}$$

where s and s^2 denote the the differential operators $\frac{d}{dx}$ and $\frac{d^2}{dx^2}$.

Assuming a solution of the form exp(sx), the characteristic equation can be written as;

$$s^4 + 2\beta s^3 + \left[-2\rho(\rho + i\gamma) + \beta^2 + \gamma^2 \frac{\kappa - 3}{\kappa + 1} \right] s^2 + \rho\beta \left(-2\rho + i\gamma \frac{8}{\kappa + 1} \right) s + \rho^2 \left(\rho^2 - 2i\rho\gamma - \gamma^2 + \beta^2 \frac{3 - \kappa}{\kappa + 1} \right) = 0 \tag{12}$$

The roots of the characteristic equation are;

$$s_1 = -\frac{1}{2}\left(\beta + \gamma\sqrt{\frac{3-\kappa}{\kappa+1}} \right) - \frac{1}{2}\sqrt{\beta^2 + 4\rho^2 + 4i\rho\left(\beta\sqrt{\frac{3-\kappa}{\kappa+1}} + \gamma \right) + \gamma^2\left(\frac{3-\kappa}{\kappa+1} \right)} \quad \Re e(s_1) < 0 \tag{13a}$$

$$s_2 = -\frac{1}{2}\left(\beta - \gamma\sqrt{\frac{3-\kappa}{\kappa+1}} \right) - \frac{1}{2}\sqrt{\beta^2 + 4\rho^2 - 4i\rho\left(\beta\sqrt{\frac{3-\kappa}{\kappa+1}} - \gamma \right) + \gamma^2\left(\frac{3-\kappa}{\kappa+1} \right)} \quad \Re e(s_2) < 0 \tag{13b}$$

$$s_3 = -\frac{1}{2}\left(\beta + \gamma\sqrt{\frac{3-\kappa}{\kappa+1}} \right) + \frac{1}{2}\sqrt{\beta^2 + 4\rho^2 + 4i\rho\left(\beta\sqrt{\frac{3-\kappa}{\kappa+1}} + \gamma \right) + \gamma^2\left(\frac{3-\kappa}{\kappa+1} \right)} \quad \Re e(s_3) > 0 \tag{13c}$$

$$s_4 = -\frac{1}{2}\left(\beta - \gamma\sqrt{\frac{3-\kappa}{\kappa+1}} \right) + \frac{1}{2}\sqrt{\beta^2 + 4\rho^2 - 4i\rho\left(\beta\sqrt{\frac{3-\kappa}{\kappa+1}} + \gamma \right) + \gamma^2\left(\frac{3-\kappa}{\kappa+1} \right)} \quad \Re e(s_4) > 0 \tag{13d}$$

After solving the equations (9a, b), $u(x, y)$ and $v(x, y)$ are written as

$$u(x,y)=\frac{1}{2\pi}\int_{-\infty}^{+\infty}\sum_{j=1}^{2}M_j(\rho)\exp(s_j x+i\rho y)\,d\rho \tag{14a}$$

$$v(x,y)=\frac{1}{2\pi}\int_{-\infty}^{+\infty}\sum_{j=1}^{2}M_j N_j(\rho)\exp(s_j x+i\rho y)\,d\rho \tag{14b}$$

Above M_j are unknown functions of ρ and

$$N_j(\rho)=\frac{(\kappa-1)\rho^2-(\kappa+1)s_j^2-\beta(\kappa+1)s_j-\gamma(\kappa-1)\rho i}{2i\rho s_j+\gamma(\kappa-1)s_j+\beta i\rho(3-\kappa)} \tag{15}$$

j=1, 2. Note that in order to ensure the regularity condition for $u(x,y)$ and $v(x,y)$, only the roots with negative real part are used.

The stresses can be obtained by substituting equations (14a), (14b) into (3a), (3b), and (3c) as follows;

$$\sigma_{xx}(x,y)=\frac{\mu(x,y)}{\kappa-1}\frac{1}{2\pi}\int_{-\infty}^{\infty}\sum_{j=1}^{2}\left[(\kappa+1)s_j+(3-\kappa)i\rho N_j\right]M_j\exp(s_j x+i\rho y)d\rho \tag{16a}$$

$$\sigma_{yy}(x,y)=\frac{\mu(x,y)}{\kappa-1}\frac{1}{2\pi}\int_{-\infty}^{\infty}\sum_{j=1}^{2}\left[(3-\kappa)s_j+(\kappa+1)i\rho N_j\right]M_j\exp(s_j x+i\rho y)d\rho \tag{16b}$$

$$\sigma_{xy}(x,y)=\mu(x,y)\int_{-\infty}^{\infty}\sum_{j=1}^{2}(i\rho+N_j s_j)M_j\exp(s_j x+i\rho y)d\rho \tag{16c}$$

The normal displacement derivative in the contact area can be written as

$$\frac{\partial u}{\partial y}(x,y)=\frac{1}{2\pi}\int_{-\infty}^{+\infty}\sum_{j=1}^{2}i\rho\,M_j\exp(s_j x+i\rho y)d\rho \tag{17}$$

In the above equations M_j is the unknown. M_j can be found by using the boundary conditions;

$$\frac{\mu(0,y)}{\kappa-1}\frac{1}{2\pi}\int_{-\infty}^{+\infty}\sum_{j=1}^{2}\left[(\kappa+1)s_j+(3-\kappa)i\rho N_j\right]M_j\exp(i\rho y)d\rho = \\ =\begin{cases} f(y) & a<y<b \\ 0 & -\infty<y<a\,,\,b<y<+\infty \end{cases} \tag{18a}$$

$$\mu(0,y)\frac{1}{2\pi}\int_{-\infty}^{+\infty}\sum_{j=1}^{2}\left(i\rho+N_j s_j\right)M_j\exp(i\rho y)d\rho = \\ =\begin{cases} \eta f(y) & a<y<b \\ 0 & -\infty<y<a\,,\,b<y<+\infty \end{cases} \tag{18b}$$

After taking inverse Fourier Transforms of both sides, we obtain

$$\sum_{j=1}^{2}\left[s_j(\kappa+1)+i\rho N_j(3-\kappa)\right]M_j=\int_a^b\frac{\kappa-1}{\mu(0,t)}f(t)\exp(-i\rho t)\,dt \tag{19a}$$

$$\sum_{j=1}^{2}\left(i\rho+N_j s_j\right)M_j=\int_a^b\frac{1}{\mu(0,t)}\eta f(t)\exp(-i\rho t)\,dt \tag{19b}$$

Thus $M_j(\rho)$, j=1,2 are given by

$$M_j=\frac{1}{\mu_0}\left[\phi_j(\rho)\int_a^b f(t)\exp[-t(i\rho+\gamma)]dt+\psi_j(\rho)\int_a^b\eta f(t)\exp[-t(i\rho+\gamma)]\,dt\right] \tag{20}$$

In equation (20) $\varphi_j(\rho)$ and $\psi(\rho)$ can be determined by using a symbolic manipulator. Substituting (20) into (17) normal displacement derivative can be written as:

$$\frac{\partial u}{\partial y}(x,y)=\frac{1}{\mu_0}\left\{\begin{array}{l}\int_a^b \exp(-\gamma t)f(t)dt\,\frac{1}{2\pi}\int_{-\infty}^{\infty}\left(i\rho\sum_{j=1}^{2}\phi_j\exp(s_j x)\right)\exp(i\rho(y-t))d\rho \\ +\int_a^b \exp(-\gamma t)\eta f(t)dt\,\frac{1}{2\pi}\int_{-\infty}^{\infty}\left(i\rho\sum_{j=1}^{2}\psi_j\exp(s_j x)\right)\exp(i\rho(y-t))d\rho\end{array}\right\} \tag{21}$$

The above equation can be simplified by introducing the following terms

$$H_{11}(\rho,x)=i\rho\sum_{j=1}^{2}\phi_j(\rho)\exp(s_j x) \tag{22a}$$

$$H_{12}(\rho,x)=i\rho\sum_{j=1}^{2}\psi_j(\rho)\exp(s_j x) \tag{22b}$$

Thus, *du/dy* becomes

$$\frac{\partial u}{\partial y}(x,y)=\frac{1}{\mu_0}\left\{\begin{array}{l}\int_a^b \exp(-\gamma t)f(t)dt\,\frac{1}{2\pi}\int_{-\infty}^{\infty}H_{11}\exp(i\rho(y-t))d\rho \\ +\int_a^b \exp(-\gamma t)\eta f(t)dt\,\frac{1}{2\pi}\int_{-\infty}^{\infty}H_{12}\exp(i\rho(y-t))d\rho\end{array}\right\} \tag{23}$$

As for the numerical solution, it is easier to deal with (0, ∞) instead of dealing with (-∞, ∞). So we convert the integrals from (-∞, ∞) to (0, ∞) as below;

$$\begin{aligned}\int_{-\infty}^{\infty}H_{11}(\rho,x)\exp(i\rho(y-t))d\rho &= \int_0^{\infty}\left[H_{11}(\rho,x)+H_{11}(-\rho,x)\right]\cos(\rho(y-t))\,d\rho \\ &+\int_0^{\infty} i\left[H_{11}(\rho,x)-H_{11}(-\rho,x)\right]\sin(\rho(y-t))\,d\rho\end{aligned} \tag{24a}$$

$$\begin{aligned}\int_{-\infty}^{\infty}H_{12}(\rho,x)\exp(i\rho(y-t))d\rho &= \int_0^{\infty}\left[H_{12}(\rho,x)+H_{12}(-\rho,x)\right]\cos(\rho(y-t))\,d\rho \\ &+\int_0^{\infty} i\left[H_{12}(\rho,x)-H_{12}(-\rho,x)\right]\sin(\rho(y-t))\,d\rho\end{aligned} \tag{24b}$$

Some of the new terms can be introduced as;

$$K_{11}(\rho,x)=H_{11}(\rho,x)+H_{11}(-\rho,x) \tag{25a}$$

$$K_{12}(\rho,x)=i\left[H_{11}(\rho,x)+H_{11}(-\rho,x)\right] \tag{25b}$$

$$K_{13}(\rho,x)=H_{12}(\rho,x)+H_{12}(-\rho,x) \tag{25c}$$

$$K_{14}(\rho,x)=i\left[H_{12}(\rho,x)-H_{12}(-\rho,x)\right] \tag{25d}$$

Then equation (23) will take the following form;

$$\frac{\partial u}{\partial y}(x,y)=\frac{1}{\mu_0}\left\{\begin{array}{l}\int_a^b \exp(-\gamma t)f(t)dt\,\frac{1}{2\pi}\int_0^\infty K_{11}(\rho,x)\cos(\rho(y-t))d\rho \\ +\int_a^b \exp(-\gamma t)f(t)dt\,\frac{1}{2\pi}\int_0^\infty K_{12}(\rho,x)\sin(\rho(y-t))d\rho \\ +\int_a^b \exp(-\gamma t)\eta f(t)dt\,\frac{1}{2\pi}\int_0^\infty K_{13}(\rho,x)\cos(\rho(y-t))d\rho \\ +\int_b^a \exp(-\gamma t)\eta f(t)dt\,\frac{1}{2\pi}\int_0^\infty K_{14}(\rho,x)\sin(\rho(y-t))d\rho\end{array}\right\} \tag{26}$$

In the derivation of above equation, an important step is to find the asymptotic values of the infinite integrals in (26). There are two reasons why we asymptotically expand the infinite integrals as $\rho\to\infty$. The first reason, the singular behavior of the integral equation and that of its solution comes from the leading term in the large ρ expansion of the kernel of the integrands (26). The second reason is to facilitate computational efficiency when we numerically solve the singular integral equation. In MAPLE it can be shown that,

$$s_1, s_2 = -\rho \quad \text{as} \quad \rho\to\infty \tag{27a}$$

By using the result above, asymptotic expressions for the mentioned functions can be written as,

$$K_{11}^{\infty}(\rho,x)=i\rho\left(\phi_1(\rho)+\phi_2(\rho)-\phi_1(-\rho)-\phi_2(-\rho)\right)\exp(-\rho\, x) \tag{27b}$$

$$K_{12}^{\infty}(\rho,x)=-\rho\left(\phi_1(\rho)+\phi_2(\rho)+\phi_1(-\rho)+\phi_2(-\rho)\right)\exp(-\rho\, x) \tag{27c}$$

$$K_{13}^{\infty}(\rho,x)=i\rho\left(\psi_1(\rho)+\psi_2(\rho)-\psi_1(-\rho)-\psi_2(-\rho)\right)\exp(-\rho\, x) \tag{27d}$$

$$K_{14}^{\infty}(\rho,x)=-\rho\left(\psi_1(\rho)+\psi_2(\rho)+\psi_1(-\rho)+\psi_2(-\rho)\right)\exp(-\rho\, x) \tag{27e}$$

Using MAPLE we have to complete the asymptotic analyses of $K_{11}^{\infty}, K_{12}^{\infty}, K_{13}^{\infty}$ and K_{14}^{∞} by expanding them into Taylor series as $\rho\to\infty$. The following results are obtained,

$$K_{11}^{\infty}=\left\{a_1+\frac{a_2}{\rho}+\frac{a_3}{\rho^2}+\ldots+\frac{a_6}{\rho^7}\right\}\exp(-\rho x) \tag{28}$$

where;

$$a_1=a_5=a_6=0 \tag{29a}$$

$$a_2=-\frac{(\kappa+1)(2\kappa-5)\gamma}{4} \tag{29b}$$

$$a_3=\frac{\left(-7\kappa-17+\kappa^3+3\kappa^2\right)\gamma\beta}{8} \tag{29c}$$

$$a_4=\frac{\left(4\gamma^2\kappa^4+36\gamma^2\kappa^2-20\gamma^2\kappa^3-52\gamma^2-12\gamma^2\kappa+13\beta^2\kappa^2+39\beta^2-9\beta^2\kappa\right)\gamma}{32}+\frac{\left(-\kappa^3\beta^2-2\kappa^4\beta^2\right)\gamma}{32} \tag{29d}$$

$$K_{12}^{\infty} = \left\{ b_1 + \frac{b_2}{\rho} + \frac{b_3}{\rho^2} + ... + \frac{b_6}{\rho^7} \right\} \exp(-\rho x) \tag{30}$$

where;

$$b_5 = b_6 = 0 \tag{31a}$$

$$b_1 = \frac{\kappa + 1}{2} \tag{31b}$$

$$b_2 = -\frac{(5 + \kappa)\beta}{4} \tag{31c}$$

$$b_3 = \frac{5}{4}\beta^2 + \gamma^2\kappa^2 - \frac{1}{2}\gamma^2\kappa - \frac{3}{2}\gamma^2 - \frac{1}{4}\gamma^2\kappa^3 \tag{31d}$$

$$b_4 = \frac{\left(-16\beta^2 + 67\gamma^2 - 25\gamma^2\kappa^2 + 3\gamma^2\kappa^3 - 7\gamma^2\kappa + 2\gamma^2\kappa^4\right)\beta}{32} \tag{31e}$$

$$K_{13}^{\infty} = \left\{ c_1 + \frac{c_2}{\rho} + \frac{c_3}{\rho^2} + ... + \frac{c_6}{\rho^7} \right\} \exp(-\rho x) \tag{32}$$

where;

$$c_5 = c_6 = 0 \tag{33a}$$

$$c_1 = \frac{-\kappa + 1}{2} \tag{33b}$$

$$c_2 = \frac{(\kappa + 1)\beta}{4} \tag{33c}$$

$$c_3 = -\frac{1}{4}\gamma^2 + \frac{1}{4}\gamma^2\kappa^3 - \frac{1}{2}\gamma^2\kappa^2 - \frac{1}{2}\beta^2 \tag{33d}$$

$$c_4 = -\frac{\left(7\gamma^2\kappa^3 - 23\gamma^2\kappa^2 - 13\gamma^2\kappa + 2\gamma^2\kappa^4 + 3\gamma^2 - 4\beta^2\right)\beta}{32} \tag{33e}$$

$$K_{14}^{\infty} = \left\{d_1 + \frac{d_2}{\rho} + \frac{d_3}{\rho^2} + ... + \frac{d_6}{\rho^7}\right\}\exp(-\rho x) \tag{34}$$

where;

$$d_1 = d_5 = d_6 = 0 \tag{35a}$$

$$d_2 = -\frac{\gamma\left(2\kappa^2 - 3\kappa - 1\right)}{4} \tag{35b}$$

$$d_3 = \frac{\gamma\left(\kappa^2 - 1 - 5\kappa + \kappa^3\right)\beta}{8} \tag{35c}$$

$$d_4 = \frac{\left(-8\gamma^2 - 12\gamma^2\kappa^3 - 12\gamma^2\kappa + 4\gamma^2\kappa^4 + 12\gamma^2\kappa^2 + 3\beta^2\kappa^3 - 2\beta^2\kappa^4 - 7\beta^2\kappa\right)\gamma}{32} + \frac{\left(7\kappa^2\beta^2 - 9\beta^2\right)\gamma}{32} \tag{35d}$$

After using the above results, equation (26) will take the below form by subtracting and adding the first terms

$$\frac{\partial u}{\partial y}(x,y)=\frac{1}{\mu_0}\left\{\begin{array}{l}\int_a^b \exp(-\gamma t)f(t)dt\,\frac{1}{2\pi}\int_0^\infty K_{11}(\rho,x)\cos(\rho(y-t))d\rho \\ +\int_a^b \exp(-\gamma t)f(t)dt\,\frac{1}{2\pi}\int_0^\infty [K_{12}(\rho,x)-b_1\exp(-\rho x)]\sin(\rho(y-t))d\rho \\ +\int_a^b \exp(-\gamma t)f(t)dt\,\frac{1}{2\pi}\int_0^\infty b_1\exp(-\rho x)\sin(\rho(y-t))d\rho \\ +\int_b^a \eta f(t)\exp(-\gamma t)dt\,\frac{1}{2\pi}\left[\int_0^\infty (K_{13}(\rho,x)-c_1\exp(-\rho x))\cos(\rho(y-t))d\rho\right] \\ +\int_b^a \eta f(t)\exp(-\gamma t)dt\,\frac{1}{2\pi}\int_0^\infty c_1\exp(-\rho x)\cos(\rho(y-t))d\rho \\ +\int_b^a \eta f(t)\exp(-\gamma t)dt\,\frac{1}{2\pi}\int_0^\infty K_{14}(\rho,x)\sin(\rho(y-t))d\rho\end{array}\right\} \quad (36)$$

We can use the following formulas to evaluate the second and third terms in closed-form

$$\int_0^\infty \exp(-\rho\, x)\cos(\rho(y-t))\,d\rho=\frac{x}{x^2+(y-t)^2} \quad (37a)$$

$$\int_0^\infty \exp(-\rho\, x)\sin(\rho(y-t))\,d\rho=\frac{y-t}{x^2+(y-t)^2} \quad (37b)$$

We can now make the following definitions

$$P_1(t)=f(t)\exp(-(\gamma+\beta)t) \quad (38)$$

$$Q_1(t)=\eta f(t)\exp(-(\gamma+\beta)t) \quad (39)$$

Substituting in (36), and taking the limit as $x\rightarrow 0$, we get;

$$\frac{\partial u(0,y)}{\partial y}=\frac{1}{2\pi\mu_o}\left\{\begin{array}{l}\dfrac{\kappa+1}{2}\displaystyle\int_a^b\frac{P_1(t)}{y-t}dt+\int_a^b P_1(t)dt\left[\int_0^\infty K_{11}(\rho,0)\cos(\rho(y-t))d\rho\right]\\ +\displaystyle\int_a^b P_1(t)dt\left[\int_0^\infty (K_{12}(\rho,0)-b_1)\sin(\rho(y-t)d\rho)\right]\\ -\dfrac{\kappa-1}{2}\pi Q_1(y)+\displaystyle\int_a^b Q_1(t)dt\left[\int_0^\infty K_{13}(\rho,0)-c_1\right]\cos(\rho(y-t)d\rho)\\ +\displaystyle\int_a^b Q_1(t)dt\left[\int_0^\infty K_{14}(\rho,0)\sin(\rho(y-t)d\rho)\right]\end{array}\right\} \tag{40}$$

After multiplying both sides of (40) by $(4\mu_0/\kappa+1)$, the below form of the equation for the displacement derivative can be obtained;

$$\left(\frac{4\mu_0}{\kappa+1}\right)\frac{\partial u(0,y)}{\partial y}=\frac{1}{\pi}\int_a^b\frac{P_1(t)}{(y-t)}dt-\left(\frac{\kappa-1}{\kappa+1}\right)Q_1(y)$$

$$+\int_a^b P_1(t)dt\left(\frac{2}{\pi(\kappa+1)}\right)\left(\int_0^\infty K_{11}(\rho,0)\cos(\rho(y-t)d\rho)+\int_0^\infty (K_{12}(\rho,0)-b_1)\sin(\rho(y-t)d\rho)\right) \tag{41}$$

$$+\int_a^b Q_1(t)dt\left(\frac{2}{\pi(\kappa+1)}\right)\left(\int_0^\infty (K_{13}(\rho,0)-c_1)\cos(\rho(y-t)d\rho)+\int_0^\infty K_{14}(\rho,0)\sin(\rho(y-t)d\rho)\right)$$

In equation (41) we have Cauchy singularities and free terms. We can make the following definitions

$$\int_0^\infty K_{11}(\rho,0)\cos(\rho(y-t))d\rho=h_{11}(y,t) \tag{42a}$$

$$\int_0^{\infty}\left(K_{12}(\rho,0)-b_1\right)\sin\left(\rho(y-t)\right)d\rho = h_{12}(y,t) \tag{42b}$$

$$\int_0^{\infty}\left(K_{13}(\rho,0)-c_1\right)\cos\left(\rho(y-t)\right)d\rho = h_{13}(y,t) \tag{42c}$$

$$\int_0^{\infty}K_{14}(\rho,0)\sin\left(\rho(y-t)\right)d\rho = h_{14}(y,t) \tag{42d}$$

In numerical computation of $h_{11}(y,t)$, $h_{12}(y,t)$, $h_{13}(y,t)$ and $h_{41}(y,t)$ integration cut-off points are used. These expressions are simplified as;

$$\begin{aligned} h_{11}(y,t) &= \int_0^{A_{11}}K_{11}(\rho,0)\cos\left(\rho(y-t)\right)d\rho + \int_{A_{11}}^{\infty}\left(K_{11}(\rho,0)-\frac{a_2}{\rho}-\ldots-\frac{a_6}{\rho^5}\right)\cos\left(\rho(y-t)\right)d\rho \\ &+ \int_{A_{11}}^{\infty}\left(\frac{a_2}{\rho}+\ldots+\frac{a_6}{\rho^5}\right)\cos\left(\rho(y-t)\right)d\rho \end{aligned} \tag{43a}$$

$$\begin{aligned} h_{12}(y,t) &= \int_0^{A_{12}}\left(K_{12}(\rho,0)-b_1\right)\sin\left(\rho(y-t)\right)d\rho \\ &+ \int_{A_{12}}^{\infty}\left(K_{12}(\rho,0)-b_1-\ldots-\frac{b_6}{\rho^5}\right)\sin\left(\rho(y-t)\right)d\rho + \int_{A_{12}}^{\infty}\left(\frac{b_2}{\rho}+\ldots+\frac{b_6}{\rho^5}\right)\sin\left(\rho(y-t)\right)d\rho \end{aligned} \tag{43b}$$

$$\begin{aligned} h_{13}(y,t) &= \int_0^{A_{13}}\left(K_{13}(\rho,0)-c_1\right)\cos\left(\rho(y-t)\right)d\rho \\ &+ \int_{A_{13}}^{\infty}\left(K_{13}(\rho,0)-c_1-\ldots-\frac{c_6}{\rho^5}\right)\cos\left(\rho(y-t)\right)d\rho + \int_{A_{13}}^{\infty}\left(\frac{c_2}{\rho}+\ldots+\frac{c_6}{\rho^5}\right)\sin\left(\rho(y-t)\right)d\rho \end{aligned} \tag{43c}$$

$$h_{14}(y,t)=\int_{0}^{A_{14}}K_{14}(\rho,0)\sin(\rho(y-t))d\rho+\int_{A_{14}}^{\infty}\left(K_{14}(\rho,0)-\frac{d_2}{\rho}-\ldots-\frac{d_6}{\rho^5}\right)\sin(\rho(y-t))d\rho$$
$$+\int_{A_{14}}^{\infty}\left(\frac{d_2}{\rho}+\ldots+\frac{d_6}{\rho^5}\right)\sin(\rho(y-t))d\rho \tag{43d}$$

In equations (43), $A_{11}, A_{12}, A_{13}, A_{14}$ are the integration cut-off points. Gauss quadrature numerical integration method is used to compute the integrals from 0…*A*. Big values of *A* will increase the numerical efforts for the computation of the second terms on the right hand sides of the equations (43a-d). So for the great values of *A,* these terms go to zero and we have less numerical computations. However the second terms on the right hand sides of the equations can be combined with the higher order of the asymptotic development, then we can choose lower values of *A*. But the second choice will pave way for the complexity of the asymptotic analysis, therefore we will neglect the second terms on the right hand sides of the equations (43a-d). The third terms can be evaluated in closed form. The evaluation of the third term can be found in Appendix. At last the final form of the normal displacement derivative takes the form as below

$$\left(\frac{4\mu_0}{\kappa+1}\right)\frac{\partial u(0,y)}{\partial y}=\frac{1}{\pi}\int_{a}^{b}\frac{P_1(t)}{(y-t)}dt-\left(\frac{\kappa-1}{\kappa+1}\right)Q_1(y)$$
$$+\left(\frac{2}{\pi(\kappa+1)}\right)\left\{\int_{a}^{b}P_1(t)[h_{11}(y,t)+h_{12}(y,t)]dt+\int_{a}^{b}Q_1(t)[h_{13}(y,t)+h_{14}(y,t)]dt\right\} \tag{44}$$

2.2 Normalization

In order to evaluate the parameters more easily, the equation (44) can be normalized by changing the variables as below

$$y = \frac{(b-a)}{2} s + \frac{(b+a)}{2} \tag{45a}$$

$$t = \frac{(b-a)}{2} r + \frac{(b+a)}{2} \tag{45b}$$

Normalized $P_1(t)$ and $Q_1(y)$can be defined as

$$P_1(t) = P_1\left(\frac{b-a}{2} r + \frac{b+a}{2}\right) = \hat{P}_1(r) \tag{46a}$$

$$Q_1(t) = Q_1\left(\frac{b-a}{2} s + \frac{b+a}{2}\right) = \hat{Q}_1(r) \tag{46b}$$

$$Q_1(y) = Q_1\left(\frac{b-a}{2} s + \frac{b+a}{2}\right) = \hat{Q}_1(s) \tag{46c}$$

The normalized non-homogeneity parameter $(\gamma+\beta)^*$ is related to the size of the contact area and can be defined as;

$$(\gamma+\beta)^* = (\gamma+\beta)(b-a) \tag{47}$$

Substituting equations (45) and (46) into equation (44), the normalized form of the equation (44) takes form as below

$$\begin{aligned}\left(\frac{4\mu_0}{\kappa+1}\right)\frac{\partial u(0,y)}{\partial y} &= \frac{1}{\pi}\int_{-1}^{1}\frac{\hat{P}_1(r)}{(s-r)}dr - \left(\frac{\kappa-1}{\kappa+1}\right)\hat{Q}_1(s) \\ &+ \left(\frac{2}{\pi(\kappa+1)}\right)\frac{(\gamma+\beta)^*}{2}\left\{\int_{-1}^{1}\hat{P}_1(r)\left[\hat{h}^*_{11}(s,r)+\hat{h}^*_{12}(s,r)\right]dr + \int_{-1}^{1}\hat{Q}_1(r)\left[\hat{h}^*_{13}(s,r)+\hat{h}^*_{14}(s,r)\right]dr\right\}\end{aligned} \tag{48}$$

$\widehat{h}_{11}^{*}(s,r),\widehat{h}_{12}^{*}(s,r),\widehat{h}_{13}^{*}(s,r)$ and $\widehat{h}_{14}^{*}(s,r)$ are the normalized form of $h_{11}(y,t),h_{12}(y,t),h_{13}(y,t)$ and $h_{14}(y,t)$. When $(\gamma+\beta)^{*}=0$, the third term in equation (48) will disappear, then the expression for homogeneous half-plane will be formed.

$$\rho=(\gamma+\beta)\alpha \tag{49}$$

By using the above transformation, $\widehat{h}_{11}^{*}(s,r),\widehat{h}_{12}^{*}(s,r),\widehat{h}_{13}^{*}(s,r)$ and $\widehat{h}_{14}^{*}(s,r)$ can be normalized differently depending on the sign of $(\gamma+\beta)$.

For $(\gamma+\beta)>0$,

$$\widehat{h}_{11}^{*}(s,r)=\int_{0}^{A_{11}^{*}}K_{11}[(\gamma+\beta)\alpha,0]\cos\left[\alpha\frac{(\gamma+\beta)^{*}}{2}(s-r)\right]d\alpha$$
$$+\int_{A_{11}^{*}}^{\infty}\left[\frac{a_{2}^{*}}{\alpha}+\ldots+\frac{a_{6}^{*}}{\alpha^{5}}\right]\cos\left[\alpha\frac{(\gamma+\beta)^{*}}{2}(s-r)\right]d\alpha \tag{50a}$$

$$\widehat{h}_{12}^{*}(s,r)=\int_{0}^{A_{12}^{*}}K_{12}[((\gamma+\beta)\alpha,0)-b_{1}]\sin\left[\alpha\frac{(\gamma+\beta)^{*}}{2}(s-r)\right]d\alpha$$
$$+\int_{A_{12}^{*}}^{\infty}\left[\frac{b_{2}^{*}}{\alpha}+\ldots+\frac{b_{6}^{*}}{\alpha^{5}}\right]\sin\left[\alpha\frac{(\gamma+\beta)^{*}}{2}(s-r)\right]d\alpha \tag{50b}$$

$$\widehat{h}_{13}^{*}(s,r)=\int_{0}^{A_{13}^{*}}K_{13}[((\gamma+\beta)\alpha,0)-c_{1}]\cos\left[\alpha\frac{(\gamma+\beta)^{*}}{2}(s-r)\right]d\alpha$$
$$+\int_{A_{13}^{*}}^{\infty}\left[\frac{c_{2}^{*}}{\alpha}+\ldots+\frac{c_{6}^{*}}{\alpha^{5}}\right]\cos\left[\alpha\frac{(\gamma+\beta)^{*}}{2}(s-r)\right]d\alpha \tag{50c}$$

$$\widehat{h}_{14}^{*}(s,r)=\int_{0}^{A_{14}^{*}}K_{14}[(\gamma+\beta)\alpha,0]\sin\left[\alpha\frac{(\gamma+\beta)^{*}}{2}(s-r)\right]d\alpha$$
$$+\int_{A_{14}^{*}}^{\infty}\left[\frac{d_{2}^{*}}{\alpha}+\ldots+\frac{d_{6}^{*}}{\alpha^{5}}\right]\sin\left[\alpha\frac{(\gamma+\beta)^{*}}{2}(s-r)\right]d\alpha \tag{50d}$$

For $(\gamma+\beta)<0$, the integration cut-off points become negative. So the normalized terms $\widehat{h}_{11}^{*}(s,r),\widehat{h}_{12}^{*}(s,r),\widehat{h}_{13}^{*}(s,r)$ and $\widehat{h}_{14}^{*}(s,r)$ can be written as;

$$\widehat{h}_{11}^{*}(s,r)=-\int_{0}^{A_{11}^{*}}K_{11}[(\gamma+\beta)\alpha,0]\cos\left[\alpha\frac{(\gamma+\beta)^{*}}{2}(s-r)\right]d\alpha$$
$$+\int_{A_{11}^{*}}^{\infty}\left[\frac{a_2^{*}}{\alpha}+...+\frac{a_6^{*}}{\alpha^{5}}\right]\cos\left[\alpha\frac{(\gamma+\beta)^{*}}{2}(s-r)\right]d\alpha \tag{50e}$$

$$\widehat{h}_{12}^{*}(s,r)=\int_{0}^{A_{12}^{*}}K_{12}[(-(\gamma+\beta)\alpha,0)-b_1]\sin\left[\alpha\frac{(\gamma+\beta)^{*}}{2}(s-r)\right]d\alpha$$
$$+\int_{A_{12}^{*}}^{\infty}\left[\frac{b_2^{*}}{\alpha}+...+\frac{b_6^{*}}{\alpha^{5}}\right]\sin\left[\alpha\frac{(\gamma+\beta)^{*}}{2}(s-r)\right]d\alpha \tag{50f}$$

$$\widehat{h}_{13}^{*}(s,r)=-\int_{0}^{A_{13}^{*}}K_{13}[((\gamma+\beta)\alpha,0)-c_1]\cos\left[\alpha\frac{(\gamma+\beta)^{*}}{2}(s-r)\right]d\alpha$$
$$-\int_{A_{13}^{*}}^{\infty}\left[\frac{c_2^{*}}{\alpha}+...+\frac{c_6^{*}}{\alpha^{5}}\right]\cos\left[\alpha\frac{(\gamma+\beta)^{*}}{2}(s-r)\right]d\alpha \tag{50g}$$

$$\widehat{h}_{14}^{*}(s,r)=-\int_{0}^{A_{14}^{*}}K_{14}[(\gamma+\beta)\alpha,0]\sin\left[\alpha\frac{(\gamma+\beta)^{*}}{2}(s-r)\right]d\alpha$$
$$-\int_{A_{14}^{*}}^{\infty}\left[\frac{d_2^{*}}{\alpha}+...+\frac{d_6^{*}}{\alpha^{5}}\right]\sin\left[\alpha\frac{(\gamma+\beta)^{*}}{2}(s-r)\right]d\alpha \tag{50h}$$

where

$$a_2^{*}=\frac{a_2}{(\gamma+\beta)},...,a_6^{*}=\frac{a_6}{(\gamma+\beta)^{5}} \tag{51a}$$

$$b_2^{*}=\frac{b_2}{(\gamma+\beta)},...,b_6^{*}=\frac{b_6}{(\gamma+\beta)^{5}} \tag{51b}$$

$$c_2^* = \frac{c_2}{(\gamma+\beta)},...,c_6^* = \frac{c_6}{(\gamma+\beta)^5} \tag{51c}$$

$$d_2^* = \frac{a_2}{(\gamma+\beta)},...,d_6^* = \frac{a_6}{(\gamma+\beta)^5} \tag{51d}$$

$$A_{1j}^* = \frac{A_{1j}}{(\gamma+\beta)} \qquad j=1,..,4 \quad \text{(note that } A_{1j}^* \text{ are positive)} \tag{51e}$$

Using the same procedure of normalization as followed above, the equilibrium equation given in equation (7) can be normalized by equation (38) as;

$$\int_a^b P_1(y)\exp[(\gamma+\beta)y]dy = -P \tag{52}$$

Here we can define another non-homogeneity parameter related to the location of the stamp as

$$(\gamma+\beta)^{**} = (\gamma+\beta)(b+a) \tag{53}$$

By using definitions in equations (45a) and (46a), non-homogeneity parameters defined in equations (47) and (53), the normalized form of the equilibrium equation can be obtained as;

$$\int_{-1}^{1} \hat{P}_1(s)\exp\frac{1}{2}[(\gamma+\beta)^* s + (\gamma+\beta)^{**}]ds = -\frac{2P}{b-a} \tag{54}$$

In this section we derived the singular integral equation and extract all the singularities that it contains. We will give a numerical solution for the problem, assuming that our density function is an infinite expansion of the Jacobi polynomials. We obtained equation (48) and (54) to solve the any types of stamp profile. By using

a collocation technique, the problem will be reduced to an infinite system of linear algebraic equations of the unknown coefficients A_n for the flat stamp profile.

CHAPTER 3

NUMERICAL SOLUTION

3.1 Flat Stamp Problem

In this chapter the stress distribution in the loaded region will be calculated.

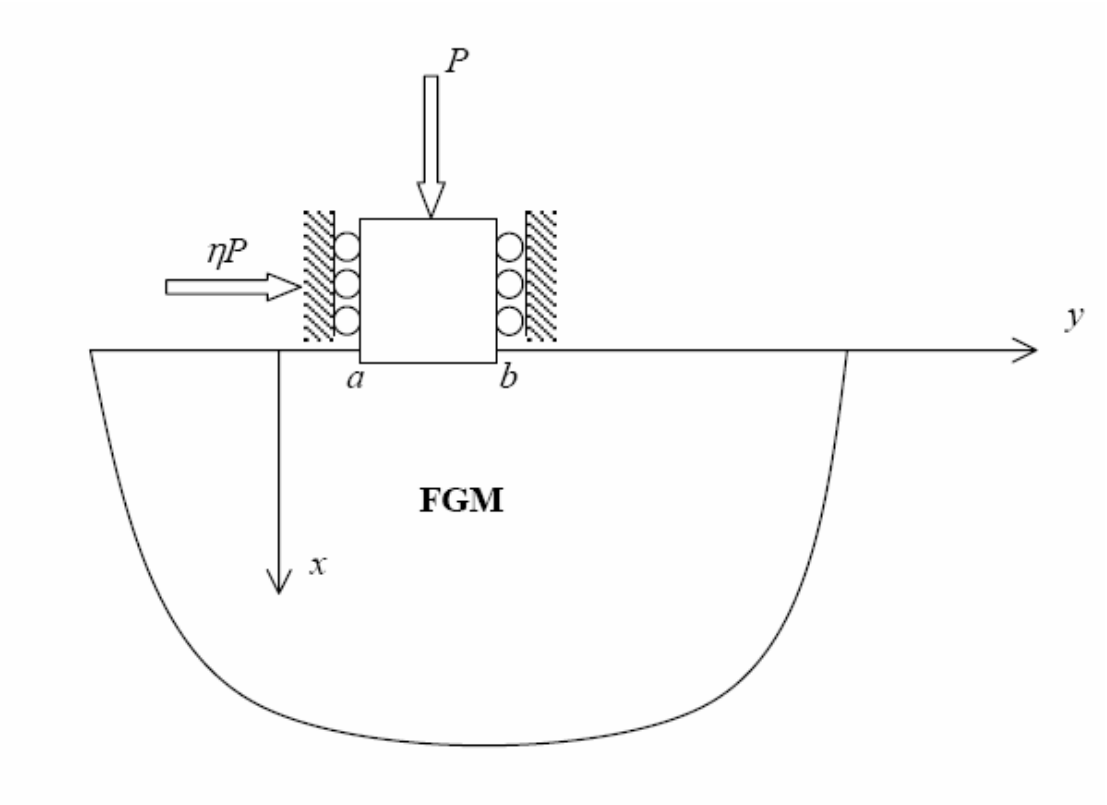

Figure 2: The general description of the contact problem for flat stamp problem

For the flat stamp problem, the displacement derivative in the contact area is constant, so we can state that

$$\frac{\partial u(0,y)}{\partial y}=0, \qquad a<y<b \tag{55}$$

$\hat{P}_1(s)$ is normalized by $P/(b-a)$. Below $\hat{P}_1(s)$ is defined as $\overline{P}_1(s)$;

$$\overline{P}_1(s)=\frac{\hat{P}_1(s)}{P/(b-a)} \tag{56}$$

By substituting equation (56) in (48) we can obtain the new version of singular integral equation as given below, note that $\overline{Q}_1(s)=\eta\overline{P}_1(s)$

$$\frac{1}{\pi}\int_{-1}^{1}\frac{\overline{P}_1(r)}{(s-r)}dr-\left(\frac{\kappa-1}{\kappa+1}\right)\eta\overline{P}_1(s)$$

$$+\left(\frac{(\gamma+\beta)^*}{\pi(\kappa+1)}\right)\left\{\int_{-1}^{1}\overline{P}_1(r)\left[\hat{h}^*{}_{11}(s,r)+\hat{h}^*{}_{12}(s,r)\right]dr+\int_{-1}^{1}\eta\overline{P}_1(r)\left[\hat{h}^*{}_{13}(s,r)+\hat{h}^*{}_{14}(s,r)\right]dr\right\}=0 \tag{57}$$

$-1<s<1$

Also we can substitute equation (56) in (54), the normalized form of the equilibrium equation becomes

$$\int_{-1}^{1}\overline{P}_1(s)\exp\frac{1}{2}\left[(\gamma+\beta)^*s+(\gamma+\beta)^{**}\right]ds=-2 \tag{58}$$

The normalized stress can now be written in the following form;

$$\overline{P}_1(r)=W_1(r)\left[\sum_{n=0}^{\infty}A_nP_n^{(\beta_1,\beta_2)}(r)\right] \tag{59}$$

where $W_1(r)$ is the weight function and defined as

$$W_1(r)=(1-r)^{\beta_1}(1+r)^{\beta_2} \tag{60}$$

A_n is the unknown constant, $P_n^{(\beta_1,\beta_2)}$ is the Jacobi polynomials, β_1 and β_2 are the strength of singularities at the ends of the contact region for the flat stamp. Here

$$\cot(\pi\beta_1)=-\eta\frac{\kappa-1}{\kappa+1} \tag{61a}$$

$$\cot(\pi\beta_2)=\eta\frac{\kappa-1}{\kappa+1} \tag{61b}$$

$$\beta_1+\beta_2=-1, \qquad -1<\beta_1<0, \qquad -1<\beta_2<0 \tag{62}$$

Above, the bounded part of the unknown function is expanded into an infinite expansion of the Jacobi polynomials. The equations (61a-b) can be derived by equation by using complex function theory. For more details on the derivation these equations, the reader may refer to Dağ [30]. By substituting equation (60) in equation (57),

$$\frac{1}{\pi}\int_{-1}^{1}\frac{W_1(r)}{s-r}\left[\sum_{n=0}^{\infty}A_nP_n^{(\beta_1,\beta_2)}(r)\right]dr-\eta\left(\frac{\kappa-1}{\kappa+1}\right)W_1(s)\left[\sum_{n=0}^{\infty}A_nP_n^{(\beta_1,\beta_2)}(s)\right]$$

$$+\left[\frac{(\gamma+\beta)^*}{\pi(\kappa+1)}\right]\left\{\int_{-1}^{1}W_1(r)\left[A_nP_n^{(\beta_1,\beta_2)}(r)\right]\left[\hat{h}_{11}^*(s,r)+\hat{h}_{12}^*(s,r)\right]dr\right\} \tag{63}$$

$$+\left[\frac{(\gamma+\beta)^*}{\pi(\kappa+1)}\right]\left\{\int_{-1}^{1}\eta W_1(r)\left[A_nP_n^{(\beta_1,\beta_2)}(r)\right]\left[\hat{h}_{13}^*(s,r)+\hat{h}_{14}^*(s,r)\right]dr\right\}=0$$

or

$$\sum_{n=0}^{\infty} A_n \left[\frac{1}{\pi} \int_{-1}^{1} \frac{W_1(r) P_n^{(\beta_1,\beta_2)}(r)}{s-r} dr - \eta \left(\frac{\kappa-1}{\kappa+1} \right) W_1(s) P_n^{(\beta_1,\beta_2)}(s) \right]$$

$$+ \sum_{n=0}^{\infty} A_n \left[\frac{(\gamma+\beta)^*}{\pi(\kappa+1)} \right] \left\{ \int_{-1}^{1} W_1(r) P_n^{(\beta_1,\beta_2)} \left[\widehat{h}_{11}^*(s,r) + \widehat{h}_{12}^*(s,r) \right] dr \right\} \tag{64}$$

$$+ \sum_{n=0}^{\infty} A_n \left[\frac{(\gamma+\beta)^*}{\pi(\kappa+1)} \right] \left\{ \int_{-1}^{1} \eta W_1(r) P_n^{(\beta_1,\beta_2)} \left[\widehat{h}_{13}^*(s,r) + \widehat{h}_{14}^*(s,r) \right] dr \right\} = 0$$

where -1<*s*<1

In equation (63) the first term can be evaluated from the properties of the Jacobi polynomials as below;

$$\frac{1}{\pi} \int_{-1}^{1} (1-r)^{\beta_1} (1+r)^{\beta_2} P_n^{(\beta_1,\beta_2)}(r) \frac{dr}{s-r} = -\cot(\pi\beta_1)(1-s)^{\beta_1} (1+s)^{\beta_2} P_n^{(\beta_1,\beta_2)}(s) + \frac{2^{-\chi}}{\sin(\pi\beta_1)} P_{n-\chi}^{(-\beta_1,-\beta_2)}(s) \tag{65}$$

where $\chi = -(\beta_1 + \beta_2) = 1$, we previously know that $\beta_1 + \beta_2 = -1$. From the equation (61a) $\cot(\pi\beta_1) = -\eta \frac{\kappa-1}{\kappa+1}$. By substituting these values the first term becomes as below;

$$\frac{1}{\pi} \int_{-1}^{1} \frac{W_1(r)}{s-r} \left[\sum_{n=0}^{\infty} A_n P_n^{(\beta_1,\beta_2)}(r) \right] dr - \eta \left(\frac{\kappa-1}{\kappa+1} \right) W_1(s) \left[\sum_{n=0}^{\infty} A_n P_n^{(\beta_1,\beta_2)}(s) \right]$$

$$= \sum_{n=1}^{\infty} A_n \begin{Bmatrix} \eta \frac{\kappa-1}{\kappa+1} (1-s)^{\beta_1} (1+s)^{\beta_2} P_n^{(\beta_1,\beta_2)} + \frac{1}{2\sin(\pi\beta_1)} P_{n-1}^{(-\beta_1,-\beta_2)} \\ -\eta \frac{\kappa-1}{\kappa+1} (1-s)^{\beta_1} (1+s)^{\beta_2} P_n^{(\beta_1,\beta_2)} \end{Bmatrix} \tag{66}$$

We rearrange equation (64) for simple calculation as

$$\sum_{n=1}^{\infty} A_n \left[\frac{1}{2\sin(\pi\beta_1)} P_{n-1}^{(-\beta_1,-\beta_2)} \right]$$

$$+ \sum_{n=0}^{\infty} A_n \left[\frac{(\gamma+\beta)^*}{\pi(\kappa+1)} \right] \left\{ \int_{-1}^{1} W_1(r) \left[P_n^{(\beta_1,\beta_2)}(r) \right] \left[\hat{h}_{11}^*(s,r) + \hat{h}_{12}^*(s,r) \right] dr \right\} \tag{67}$$

$$+ \sum_{n=0}^{\infty} A_n \left[\frac{(\gamma+\beta)^*}{\pi(\kappa+1)} \right] \left\{ \int_{-1}^{1} \eta W_1(r) \left[P_n^{(\beta_1,\beta_2)}(r) \right] \left[\hat{h}_{13}^*(s,r) + \hat{h}_{14}^*(s,r) \right] dr \right\} = 0$$

where -1<*s*<1

$$Z_{1n}(s,r) = W_1(r) P_n^{(\beta_1,\beta_2)}(r) \left[\hat{h}_{11}^*(s,r) + \hat{h}_{12}^*(s,r) \right] \tag{68a}$$

$$Z_{2n}(s,r) = \eta W_1(r) P_n^{(\beta_1,\beta_2)}(r) \left[\hat{h}_{13}^*(s,r) + \hat{h}_{14}^*(s,r) \right] \tag{68b}$$

Now equation (67) can be written as

$$\begin{aligned} &\sum_{n=1}^{\infty} A_n \left[\frac{1}{2\sin(\pi\beta_1)} P_{n-1}^{(-\beta_1,-\beta_2)} \right] \\ &+ \sum_{n=0}^{\infty} A_n \left[\frac{(\gamma+\beta)^*}{\pi(\kappa+1)} \right] \left\{ \int_{-1}^{1} Z_{1n}(s,r) dr \right\} + \sum_{n=0}^{\infty} A_n \left[\frac{(\gamma+\beta)^*}{\pi(\kappa+1)} \right] \left\{ \int_{-1}^{1} Z_{2n}(s,r) dr \right\} = 0 \end{aligned} \tag{69}$$

where -1<*s*<1

$$m_{1n}(s) = \frac{1}{2\sin(\pi\beta_1)} P_{n-1}^{(-\beta_1,-\beta_2)}(s) \tag{70a}$$

$$m_{2n}(s) = \left[\frac{(\gamma+\beta)^*}{\pi(\kappa+1)} \right] \left[\int_{-1}^{1} Z_{1n}(s,r) dr + \int_{-1}^{1} Z_{2n}(s,r) dr \right] \tag{70b}$$

As for the normalized form of the equilibrium equation, substitute equation (59) in (58)

$$\sum_{n=0}^{\infty}\int_{-1}^{1} W_1(s)A_n P_n^{(\beta_1,\beta_2)}(s)\exp\left\{\frac{1}{2}\left[(\gamma+\beta)^{*}s+(\gamma+\beta)^{**}\right]\right\}ds=-2 \tag{71}$$

We rename the above term as

$$m_{3n}=\int_{-1}^{1} W_1(s)P_n^{(\beta_1,\beta_2)}(s)\exp\left\{\frac{1}{2}\left[(\gamma+\beta)^{*}s+(\gamma+\beta)^{**}\right]\right\}ds \tag{72}$$

Finally we can write equation (69) as

$$\sum_{n=1}^{\infty}A_n m_{1n}(s)+\sum_{n=0}^{\infty}A_n m_{2n}(s)=0 \tag{73a}$$

and equation (71) can also be written as

$$\sum_{n=0}^{\infty}A_n m_{3n}=-2 \tag{73b}$$

Note that the expansion of the solution as an infinite series of Jacobi polynomials may converge to the exact solution within a few terms of the expansion. In order to deal with a finite number of unknowns, Equations (73a) and (73b) are truncated at an order $n=N$. So, we can write

$$\sum_{n=1}^{N}A_n m_{1n}(s)+\sum_{n=0}^{N}A_n m_{2n}(s)=0 \tag{74a}$$

$$\sum_{n=0}^{N}A_n m_{3n}=-2 \tag{74b}$$

Equations (74a, b) are a set of two linear equations with $N+1$ unknowns which are $A_n,(n=0\ldots N)$. In order to be able to determine these functional equations equation (74a) is collocated at N points. These points are chosen as the roots of the Chebyshev polynomials and defined as follows

$$s_i = \cos\left(\frac{\pi(2i-1)}{2N}\right) \quad ; \quad i = 1 \ldots N \tag{75}$$

Thus, we have $N+1$ equations for $N+1$ unknowns with collocation equation (74a) at N points using (75) and equation (74b). First of all the A_n , $n = 0 \ldots N$ are obtained, then the final expression of the normalized stress field is obtained by equation (59), so in order to calculate the normalized contact stress distribution $\overline{P}_1(s)$ for -1<*s*<1, a computer program is written by using Visual Fortran language. Results are in the next chapter.

3.2 Closed Form Solution of the Contact Mechanics Problem for the Homogeneous Half-Plane

In this study, a numerical solution is developed to examine the contact mechanics problem for the nonhomogeneous elastic medium. However we need to check the results of the numerical solution for contact mechanics problem for the homogeneous elastic medium. So we will calculate the contact stress distribution on the surface using the closed form solution for a homogeneous half plane in order to compare to the results of the nonhomogeneous elastic half plane. On the contrary of the nonhomogeneous elastic half plane solution, in homogeneous half plane case we take

$$(\gamma + \beta) = (\gamma + \beta)^* = (\gamma + \beta)^{**} = 0 \tag{76}$$

When we apply the condition in equation (76), equation (57) and (58) take the form:

$$\frac{1}{\pi}\int_{-1}^{1} \frac{\overline{P}_1(r)}{(s-r)}\,dr - \left(\frac{\kappa-1}{\kappa+1}\right)\eta\overline{P}_1(s) = 0 \qquad \text{, } -1<s<1 \tag{77}$$

$$\int_{-1}^{1} \overline{P}_1(s)\,ds = -2 \tag{78}$$

$$\overline{P}_1(s) = \frac{\sigma_{xx}\left(0, \frac{b-a}{2}s + \frac{b+a}{2}\right)}{P/(b-a)} \tag{79}$$

The normalized stress takes the form as

$$\overline{P}_1(s) = (1-s)^{\beta_1}(1+s)^{\beta_2}\left[\sum_{n=0}^{\infty} A_n P_n^{(\beta_1,\beta_2)}(s)\right] \tag{80}$$

where β_1 and β_2 are given by equation (61). By substituting equation (80) in (77) and integrating it in closed form using equation (65), we obtain

$$\sum_{n=1}^{\infty} A_n\left[\frac{1}{2\sin(\pi\beta_1)} P_{n-1}^{(-\beta_1,-\beta_2)}(s)\right] = 0 \tag{81}$$

The above equation is valid when

$$A_1 = A_2 = \ldots = A_n = 0 \tag{82}$$

The nonzero constant in equation (80) is A_0, so the normalized stress takes the form as

$$\overline{P}_1(s) = A_0(1-s)^{\beta_1}(1+s)^{\beta_2} \tag{83}$$

If the equation (83) is applied to equation (78), normalized form of the equilibrium equation takes the form as

$$A_0 \int_{-1}^{1} (1-s)^{\beta_1}(1+s)^{\beta_2} ds = -2 \tag{84}$$

So,

$$A_0 = \frac{2\sin(\pi\beta_2)}{\pi} \tag{85}$$

At last the normalized stress distribution for the closed form of homogeneous half plane is obtained as,

$$\overline{P}_1(s) = \frac{2\sin(\pi\beta_2)}{\pi}(1-s)^{\beta_1}(1+s)^{\beta_2} \qquad , -1<s<1 \tag{86}$$

From the equation (62) β_2 is negative. If we calculate the equation (86), we can find that the normalized stress $\overline{P}_1(s)$ is negative at every point in the contact region, thus we can easily see that the contact stresses in the contact region are compressive.

CHAPTER 4

RESULTS & CONCLUSIONS

In this chapter the numerical results and conclusions are presented. First of all the accuracy of results is checked by comparing the results for the graded medium with small nonhomogenity constant $(\gamma+\beta)^* = 0.002$ to the closed-form solution for a homogenous medium. Afterwards a detailed parametric study is done to examine effect of the nonhomogeneity parameter and the friction coefficient. As mentioned before, because the main the interest of the study is the effect of the nonhomogenity constant on the contact stress distribution, κ is fixed to a constant a value 2.

4.1 Comparisons of the Results to the Closed Form Solution

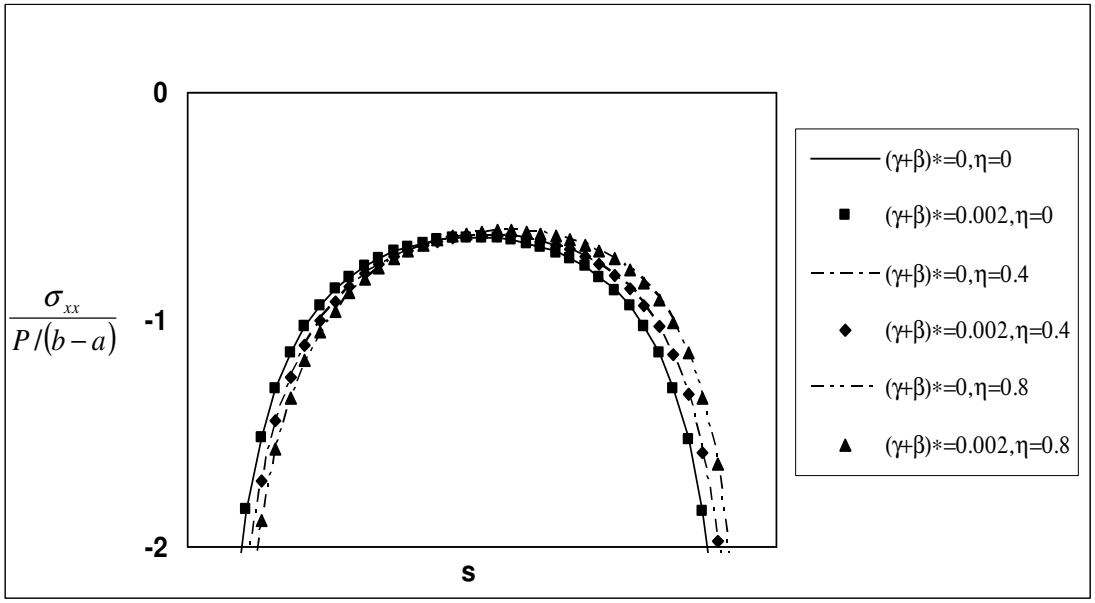

Figure 3: Comparison of the contact stress distribution to closed-form solution for various values of the friction coefficient

4.1.1 Comments on Comparisons of the Results to the Closed Form Solution

As can be seen in figure 3, the accuracy of results was checked by comparing the results obtained form the computer program when setting $(\gamma+\beta)^* = 0.002$ and the results obtained from the closed-form solution by using the expressions in 3.2 for various values of the friction coefficient. The graphs show that the results obtained by computer program are very close to the results obtained by using the closed form solutions.

Also the effects of the of the friction coefficient on the stress distribution in the loaded region can be observed. The stress distribution is symmetric about $s = 0$ for zero values of η which means that no shear stress is applied, however stress distribution in the contact area is not symmetric for the positive values of the friction coefficient (η>0). This non- symmetric form shows that the normal stress is increased in the front half of the punch and decreased in the rear part of the punch. In other words the stress distribution is increased near $s = -1$ and decreased near $s = 1$.

4.2 Parametric Studies

In the parametric analyses conducted in the present study following nonhomogeneity constants are used:

$$\gamma^* = \gamma(b-a)$$

$$\gamma^{**} = \gamma(b+a)$$

$$\beta^* = \beta(b-a)$$

$$\beta^{**} = \beta(b+a)$$

The results are given in figures between 4 and 38.

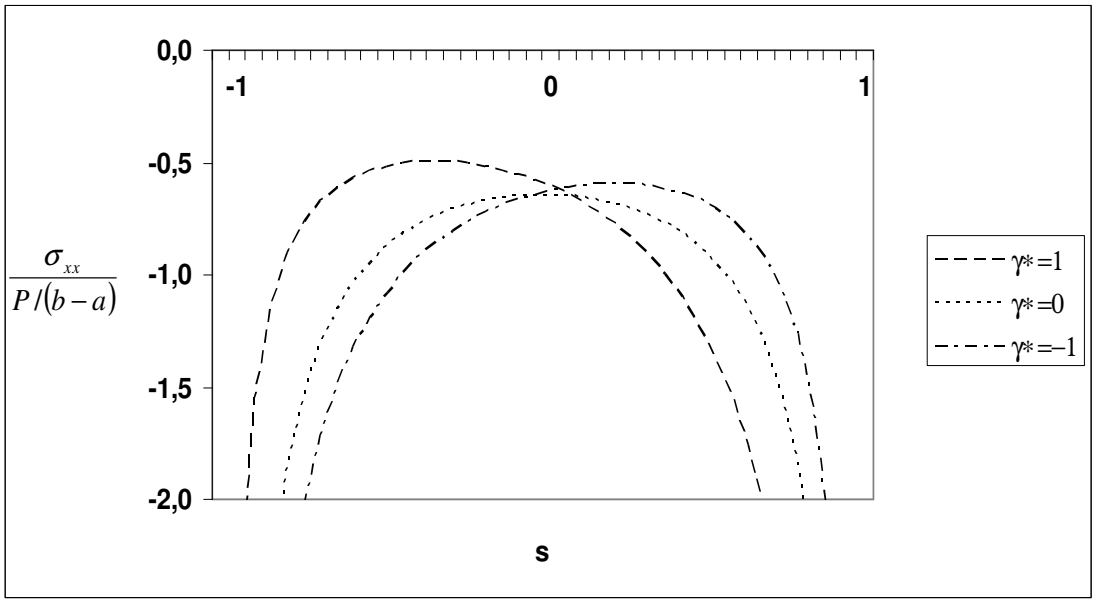

Figure 4: Normalized stress distribution for various values of the nonhomogeneity constant $\gamma\,(b\text{-}a) = \gamma^*$ [$\eta = 0$, $\beta\,(b\text{-}a) = \beta^* = \gamma\,(b\text{+}a) = \gamma^{**} = \beta\,(b\text{+}a) = \beta^{**} = 0$]

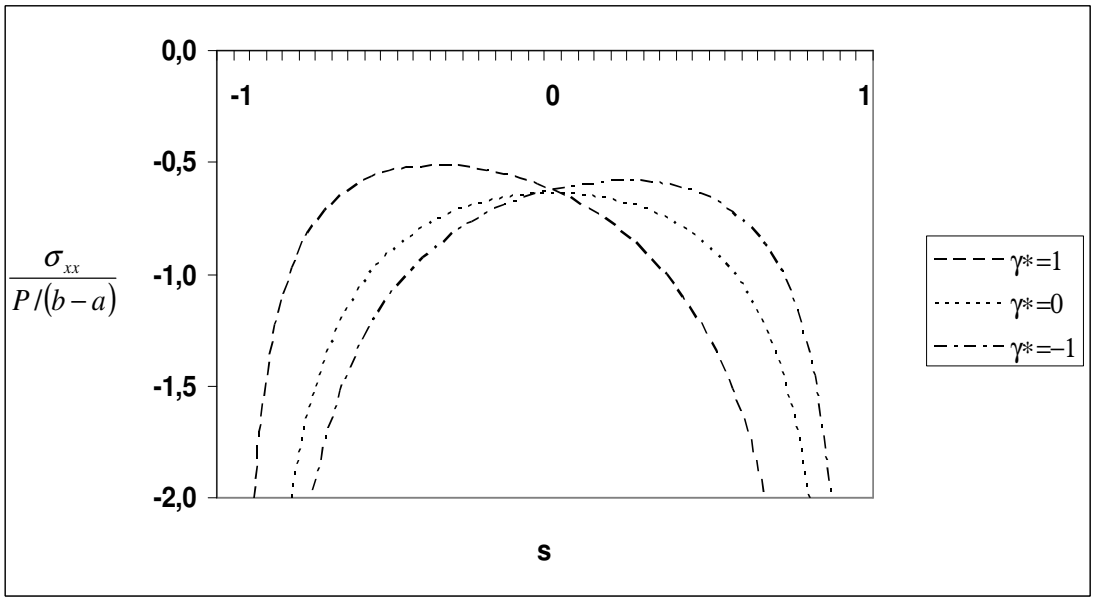

Figure 5: Normalized stress distribution for various values of the nonhomogeneity constant $\gamma\,(b\text{-}a) = \gamma^*$ [$\eta = 0.2$, $\beta\,(b\text{-}a) = \beta^* = \gamma\,(b\text{+}a) = \gamma^{**} = \beta\,(b\text{+}a) = \beta^{**} = 0$]

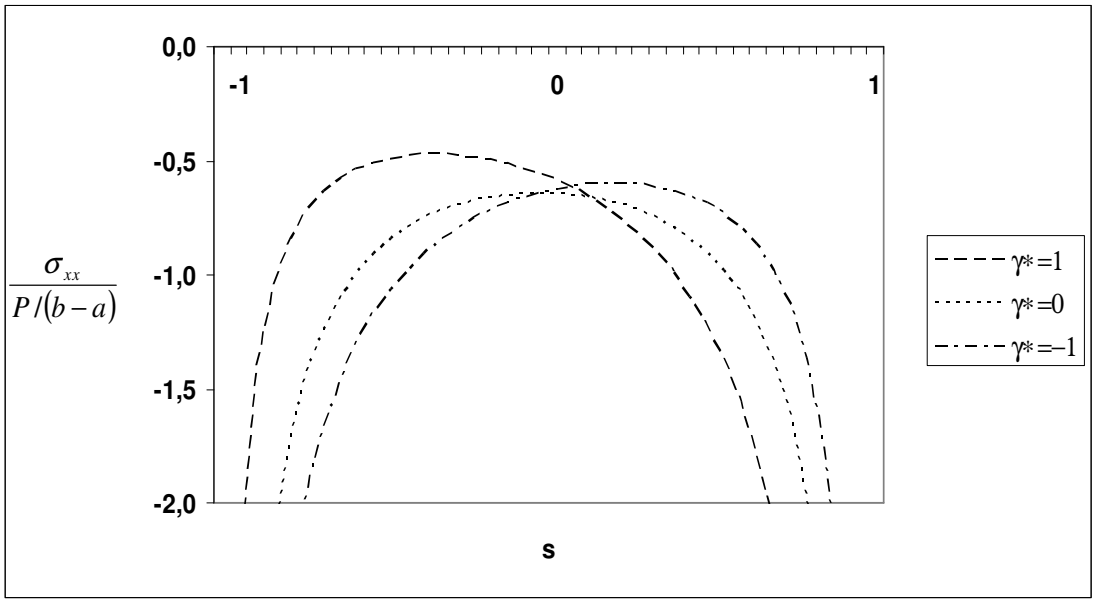

Figure 6: Normalized stress distribution for various values of the nonhomogeneity constant $\gamma\,(b\text{-}a) = \gamma^*$ [η = -0.2, $\beta\,(b\text{-}a) = \beta^* = \gamma\,(b\text{+}a) = \gamma^{**} = \beta\,(b\text{+}a) = \beta^{**} = 0$]

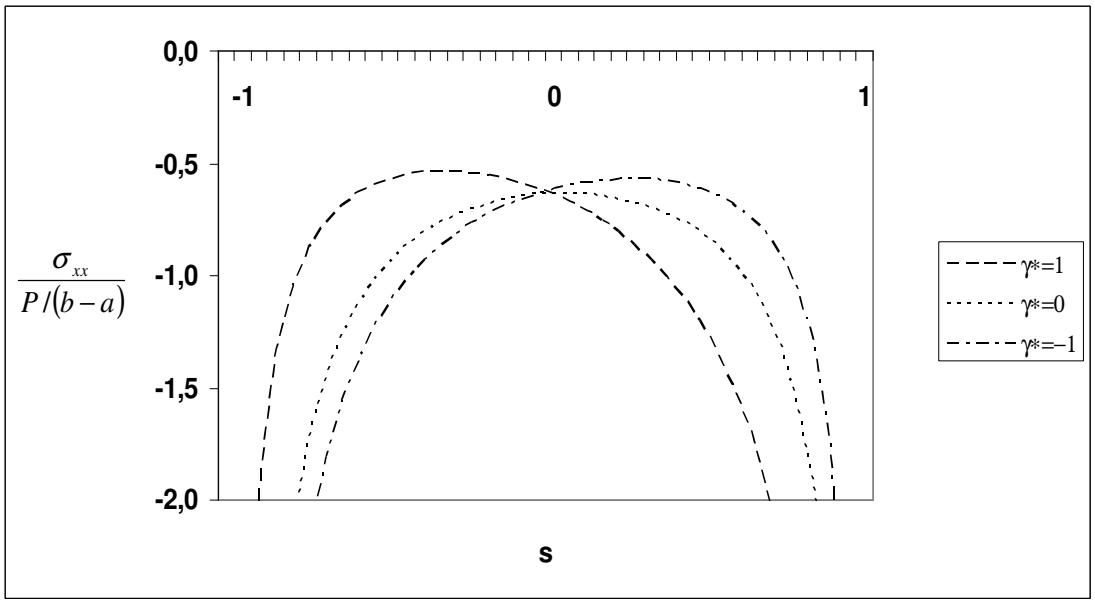

Figure 7: Normalized stress distribution for various values of the nonhomogeneity constant $\gamma\,(b\text{-}a) = \gamma^*$ [η = 0.4, $\beta\,(b\text{-}a) = \beta^* = \gamma\,(b\text{+}a) = \gamma^{**} = \beta\,(b\text{+}a) = \beta^{**} = 0$]

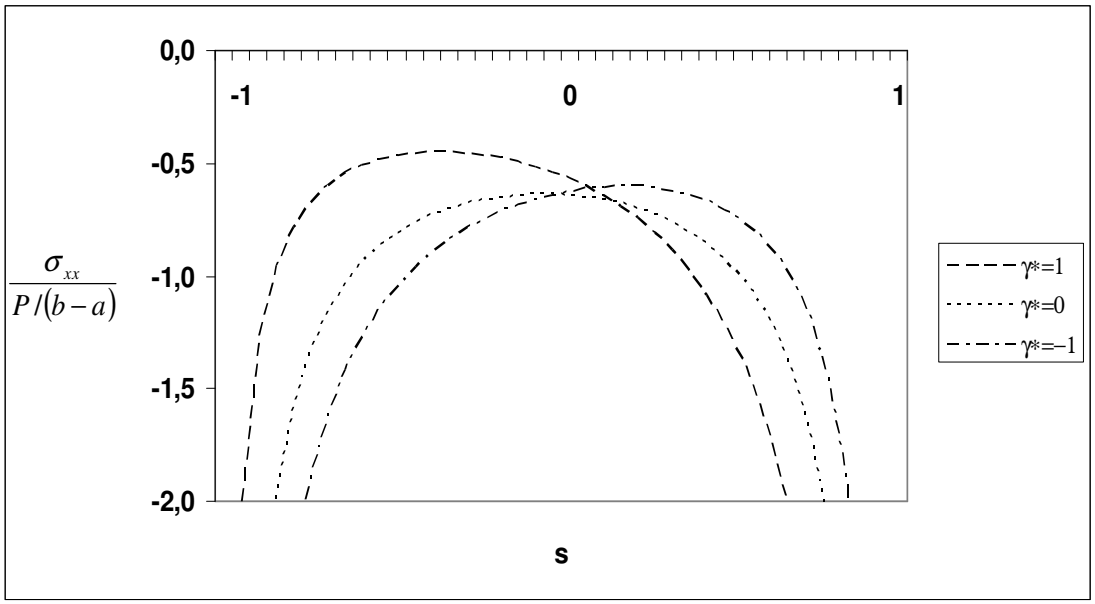

Figure 8: Normalized stress distribution for various values of the nonhomogeneity constant $\gamma (b\text{-}a) = \gamma^*$ [η = -0.4, $\beta (b\text{-}a) = \beta^* = \gamma (b+a) = \gamma^{**} = \beta (b+a) = \beta^{**} = 0$]

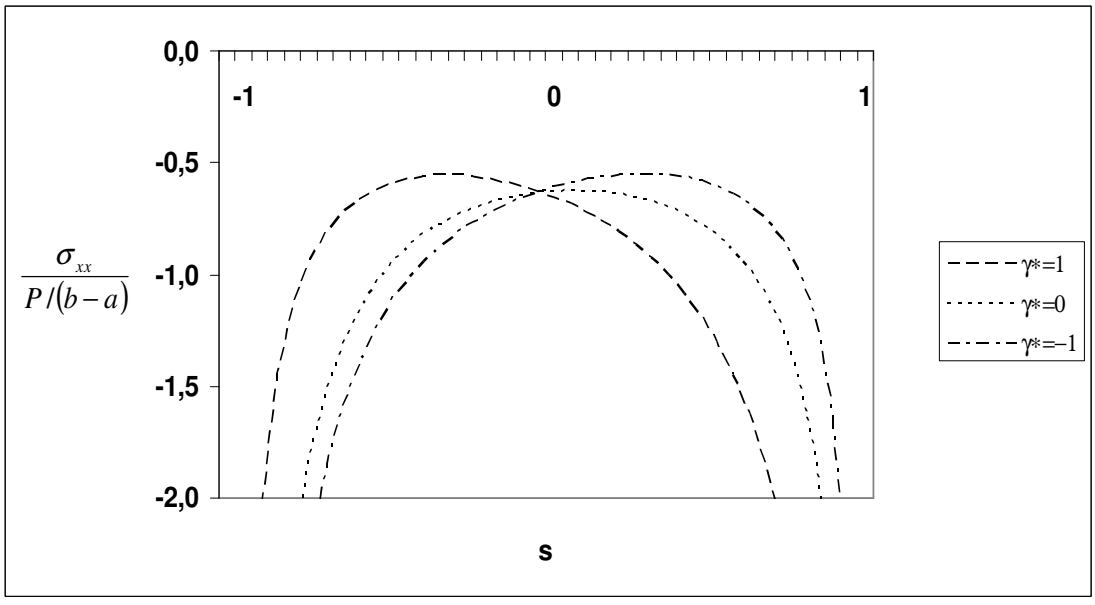

Figure 9: Normalized stress distribution for various values of the nonhomogeneity constant $\gamma (b\text{-}a) = \gamma^*$ [η = 0.6, $\beta (b\text{-}a) = \beta^* = \gamma (b+a) = \gamma^{**} = \beta (b+a) = \beta^{**} = 0$]

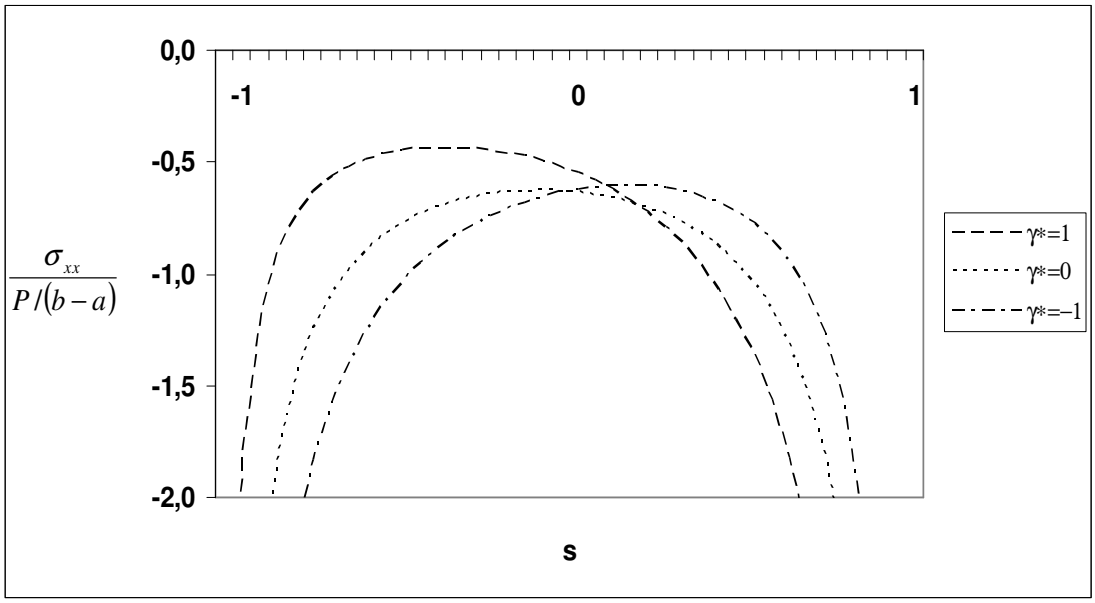

Figure 10: Normalized stress distribution for various values of the nonhomogeneity constant $\gamma\,(b\text{-}a) = \gamma^*$ [η = -0.6, $\beta\,(b\text{-}a) = \beta^* = \gamma\,(b+a) = \gamma^{**} = \beta\,(b+a) = \beta^{**} = 0$]

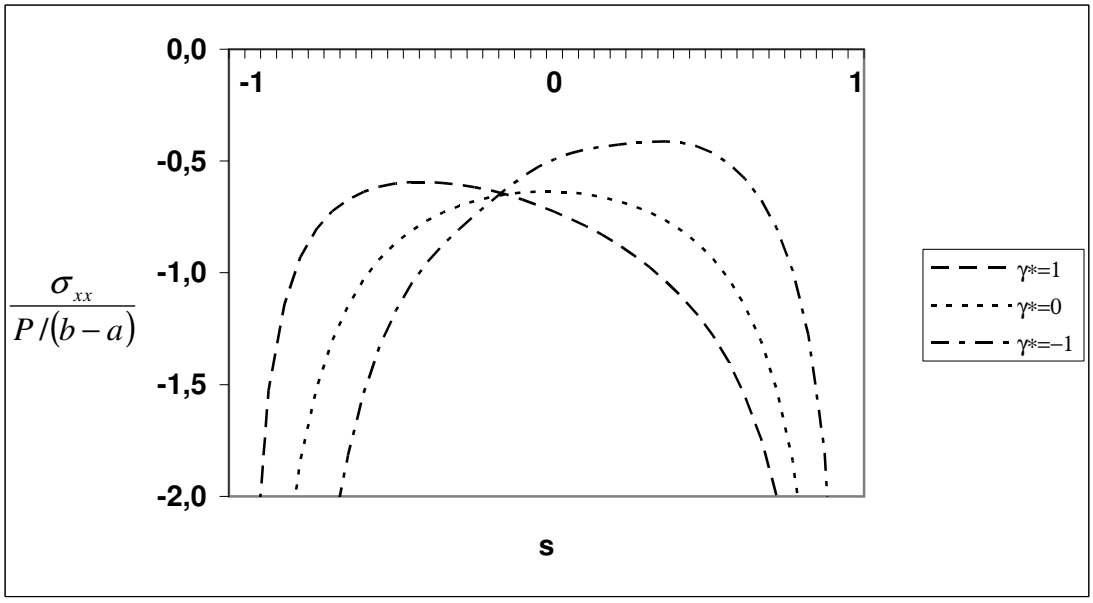

Figure 11: Normalized stress distribution for various values of the nonhomogeneity constant $\gamma\,(b\text{-}a) = \gamma^*$ [η = 0, $\beta\,(b\text{-}a) = \beta^* = 1$ and $\gamma\,(b+a) = \gamma^{**} = \beta\,(b+a) = \beta^{**} = 0$]

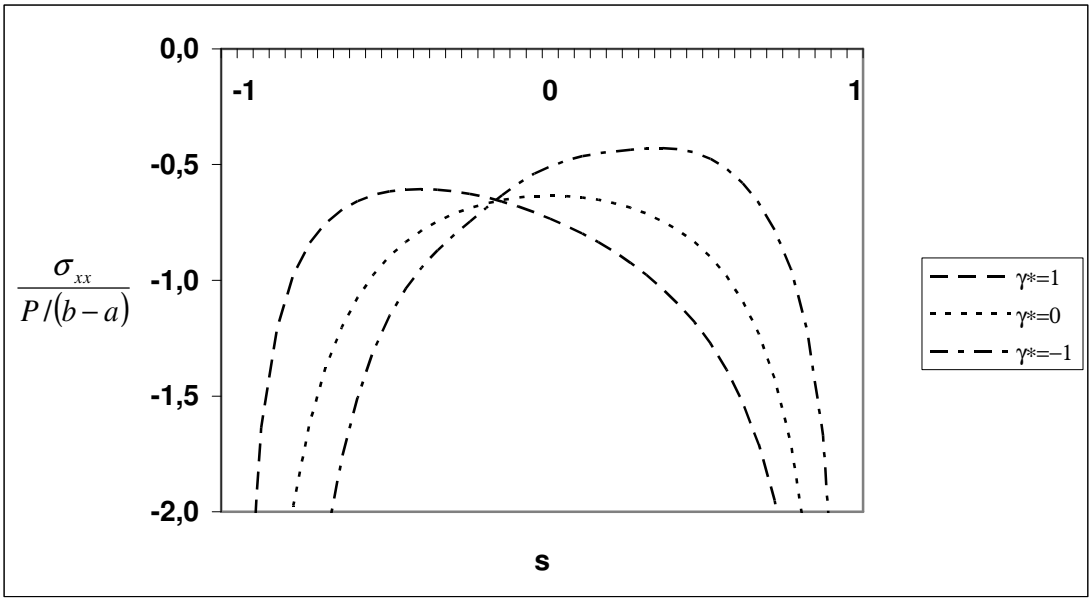

Figure 12: Normalized stress distribution for various values of the nonhomogeneity constant $\gamma\,(b\text{-}a) = \gamma^*$ [η = 0.2, $\beta\,(b\text{-}a) = \beta^* = 1$ and $\gamma\,(b\text{+}a) = \gamma^{**} = \beta\,(b\text{+}a) = \beta^{**} = 0$]

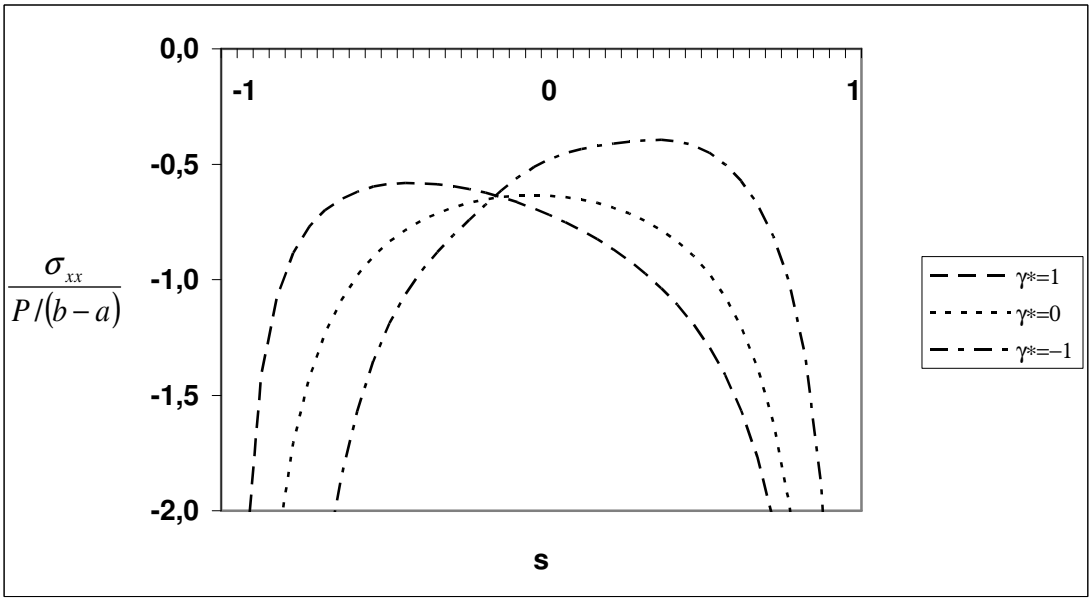

Figure 13: Normalized stress distribution for various values of the nonhomogeneity constant $\gamma\,(b\text{-}a) = \gamma^*$ [η = -0.2, $\beta\,(b\text{-}a) = \beta^* = 1$ and $\gamma\,(b\text{+}a) = \gamma^{**} = \beta\,(b\text{+}a) = \beta^{**} = 0$]

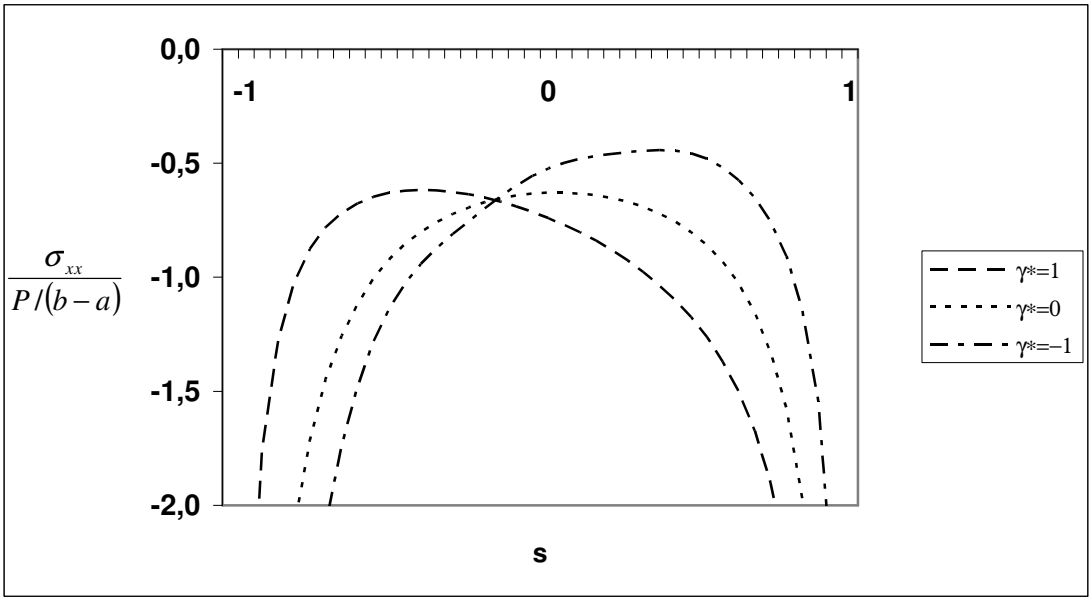

Figure 14: Normalized stress distribution for various values of the nonhomogeneity constant $\gamma\,(b\text{-}a) = \gamma^*$ [η = 0.4, $\beta\,(b\text{-}a) = \beta^* = 1$ and $\gamma\,(b\text{+}a) = \gamma^{**} = \beta\,(b\text{+}a) = \beta^{**} = 0$]

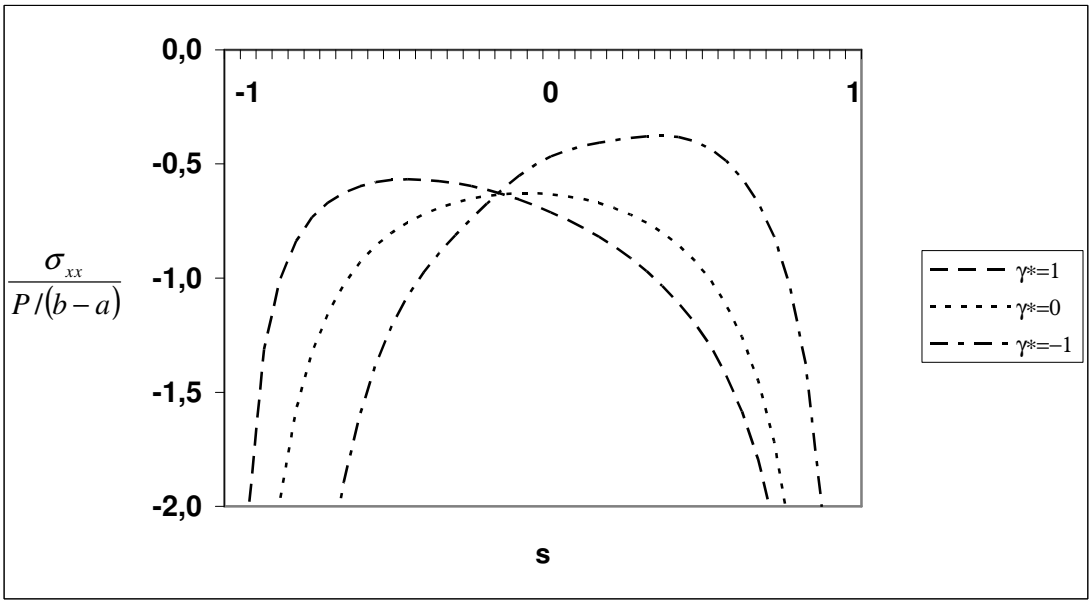

Figure 15: Normalized stress distribution for various values of the nonhomogeneity constant $\gamma\,(b\text{-}a) = \gamma^*$ [η = -0.4, $\beta\,(b\text{-}a) = \beta^* = 1$ and $\gamma\,(b\text{+}a) = \gamma^{**} = \beta\,(b\text{+}a) = \beta^{**} = 0$]

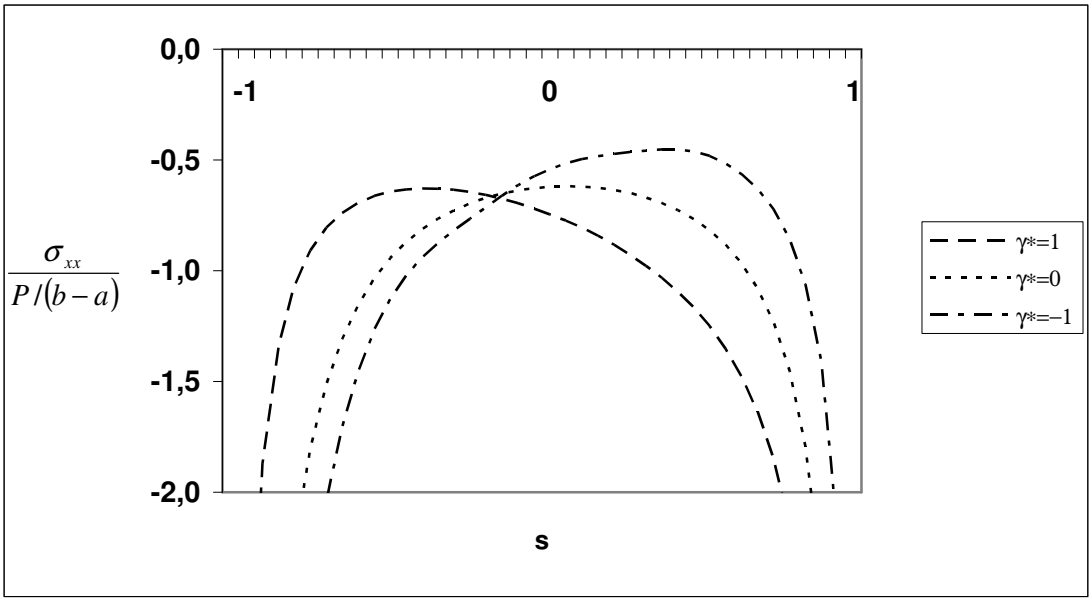

Figure 16: Normalized stress distribution for various values of the nonhomogeneity constant $\gamma\,(b\text{-}a) = \gamma^*$ [η = 0.6, $\beta\,(b\text{-}a) = \beta^* = 1$ and $\gamma\,(b\text{+}a) = \gamma^{**} = \beta\,(b\text{+}a) = \beta^{**} = 0$]

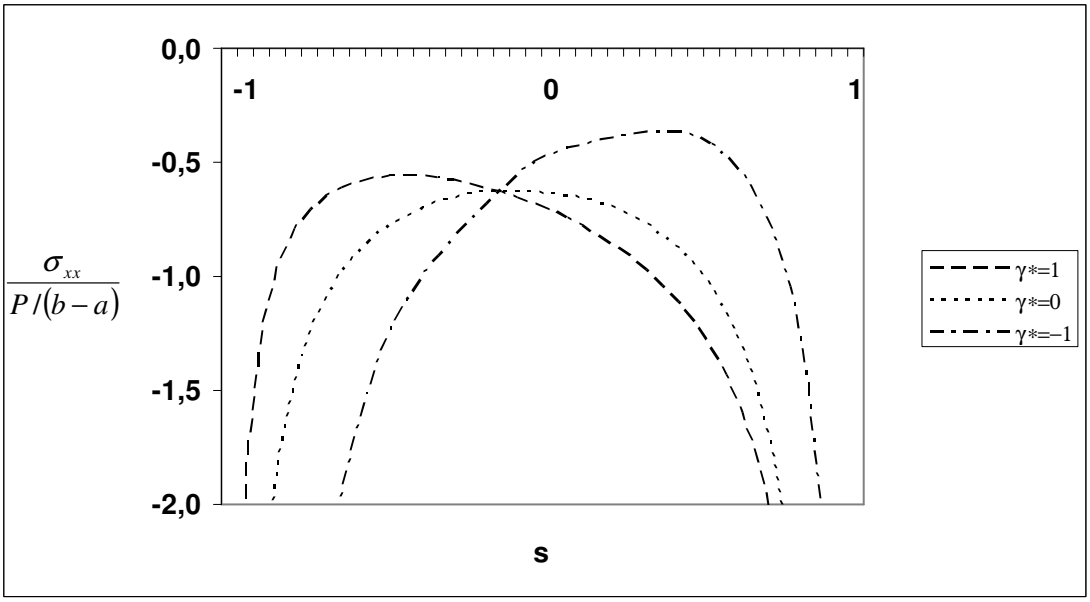

Figure 17: Normalized stress distribution for various values of the nonhomogeneity constant $\gamma\,(b\text{-}a) = \gamma^*$ [η = -0.6, $\beta\,(b\text{-}a) = \beta^* = 1$ and $\gamma\,(b\text{+}a) = \gamma^{**} = \beta\,(b\text{+}a) = \beta^{**} = 0$]

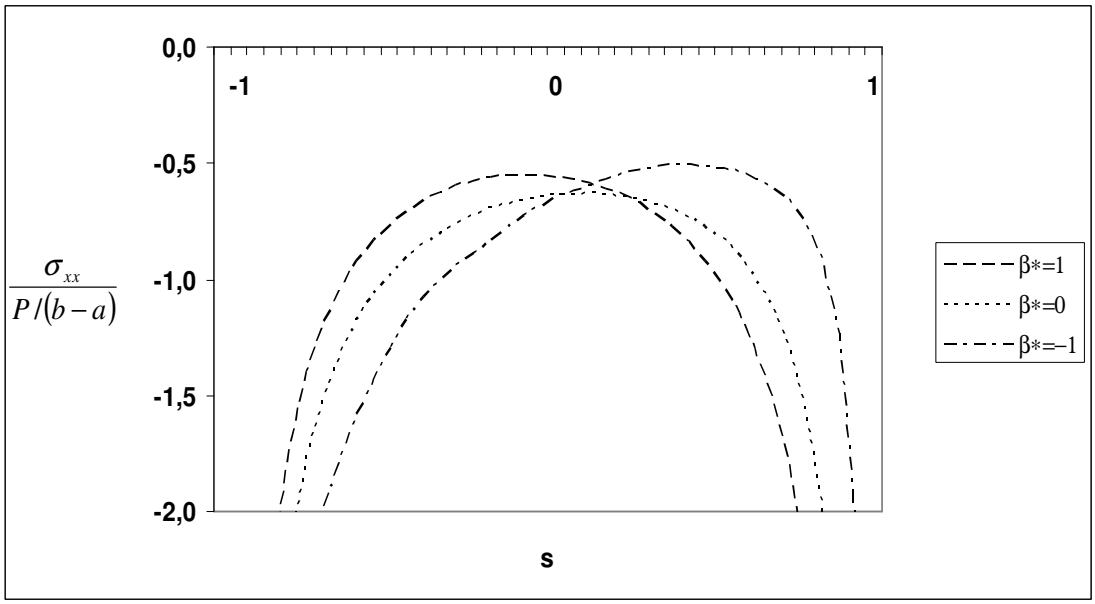

Figure 18: Normalized stress distribution for various values of the nonhomogeneity constant $\beta\,(b\text{-}a) = \beta^*$ [$\eta = 0$, $\gamma\,(b\text{-}a) = \gamma^* = -0.5$ and $\gamma\,(b\text{+}a) = \gamma^{**} = \beta\,(b\text{+}a) = \beta^{**} = 0$]

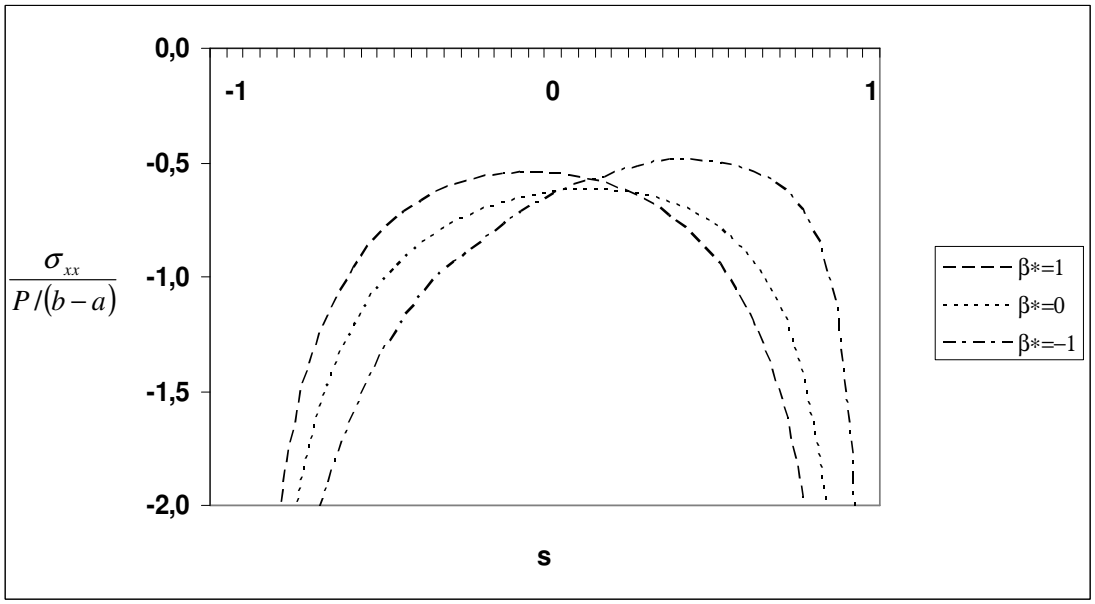

Figure 19: Normalized stress distribution for various values of the nonhomogeneity constant $\beta\,(b\text{-}a) = \beta^*$ [$\eta = 0.2$, $\gamma\,(b\text{-}a) = \gamma^* = -0.5$ and $\gamma\,(b\text{+}a) = \gamma^{**} = \beta\,(b\text{+}a) = \beta^{**} = 0$]

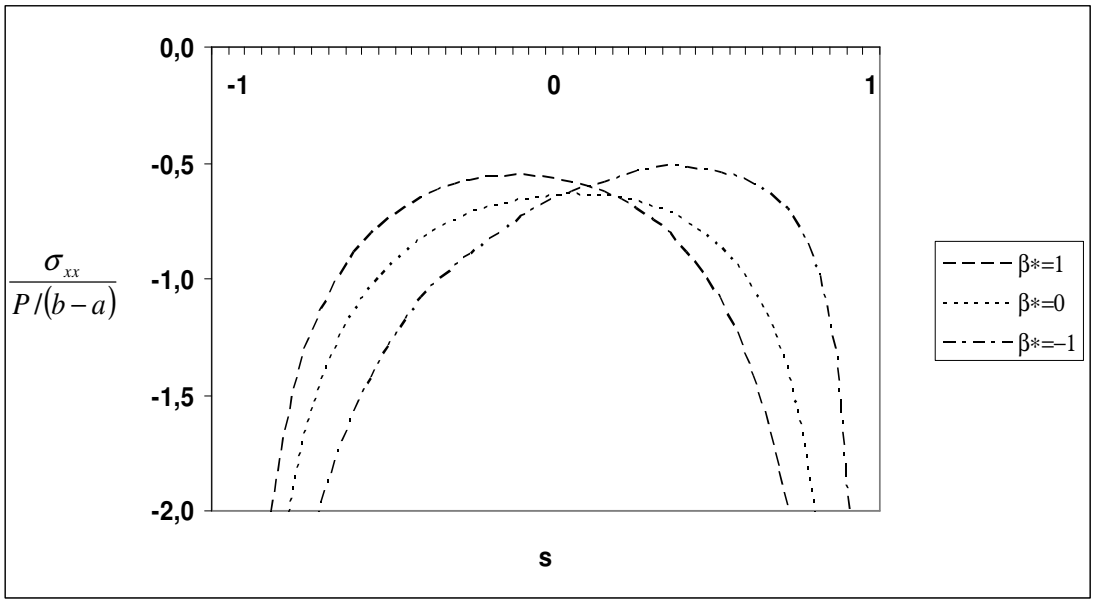

Figure 20: Normalized stress distribution for various values of the nonhomogeneity constant $\beta\,(b\text{-}a) = \beta^*$ [η = -0.2, $\gamma\,(b\text{-}a) = \gamma^*$ = -0.5 and $\gamma\,(b\text{+}a) = \gamma^{**} = \beta\,(b\text{+}a) = \beta^{**}$ =0]

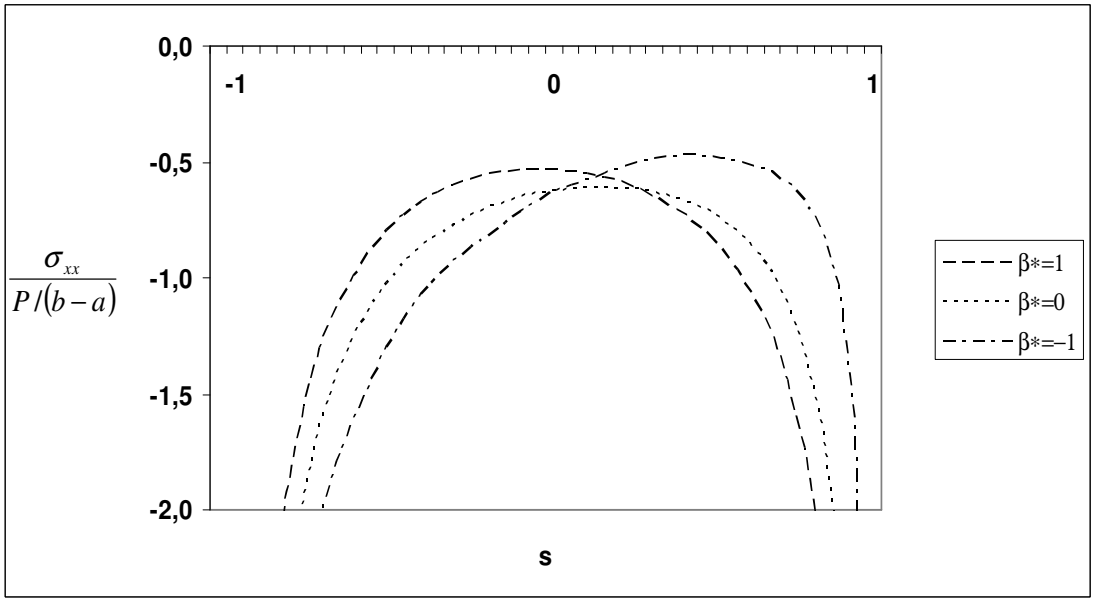

Figure 21: Normalized stress distribution for various values of the nonhomogeneity constant $\beta\,(b\text{-}a) = \beta^*$ [η = 0.4, $\gamma\,(b\text{-}a) = \gamma^*$ = -0.5 and $\gamma\,(b\text{+}a) = \gamma^{**} = \beta\,(b\text{+}a) = \beta^{**}$ =0]

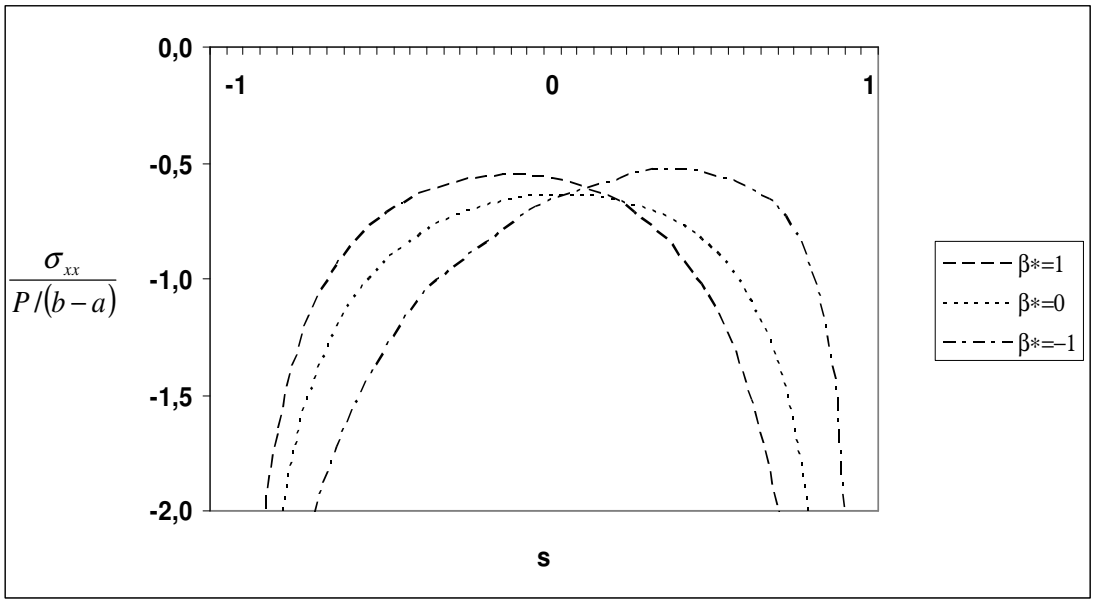

Figure 22: Normalized stress distribution for various values of the nonhomogeneity constant $\beta\,(b\text{-}a) = \beta^*$ [η = -0.4, $\gamma\,(b\text{-}a) = \gamma^*$ = -0.5 and $\gamma\,(b\text{+}a) = \gamma^{**} = \beta\,(b\text{+}a) = \beta^{**}$ =0]

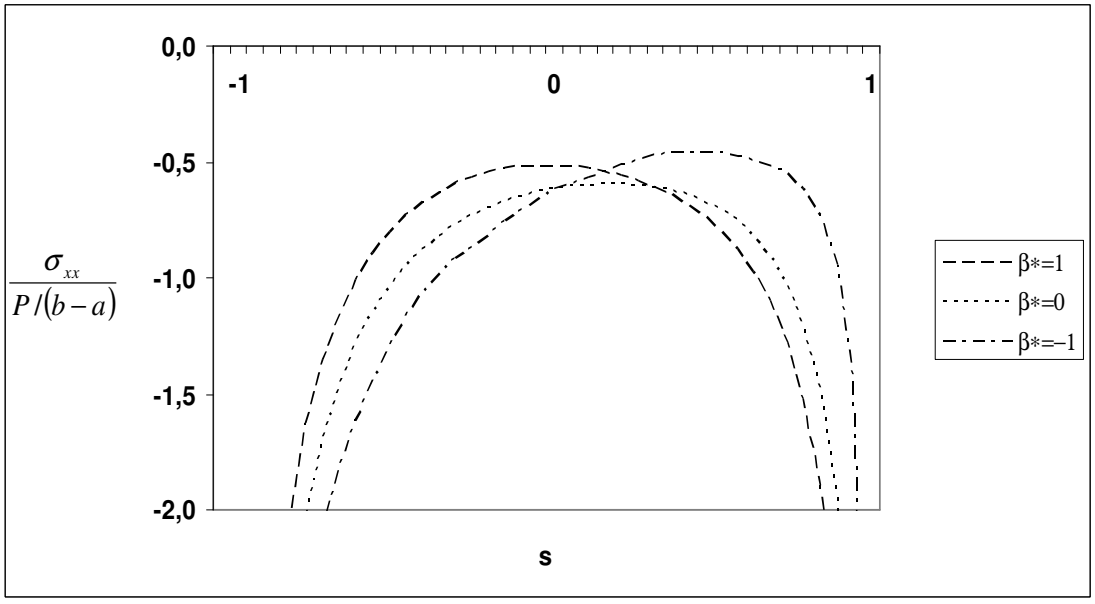

Figure 23: Normalized stress distribution for various values of the nonhomogeneity constant $\beta\,(b\text{-}a) = \beta^*$ [η = 0.6, $\gamma\,(b\text{-}a) = \gamma^*$ = -0.5 and $\gamma\,(b\text{+}a) = \gamma^{**} = \beta\,(b\text{+}a) = \beta^{**}$ =0]

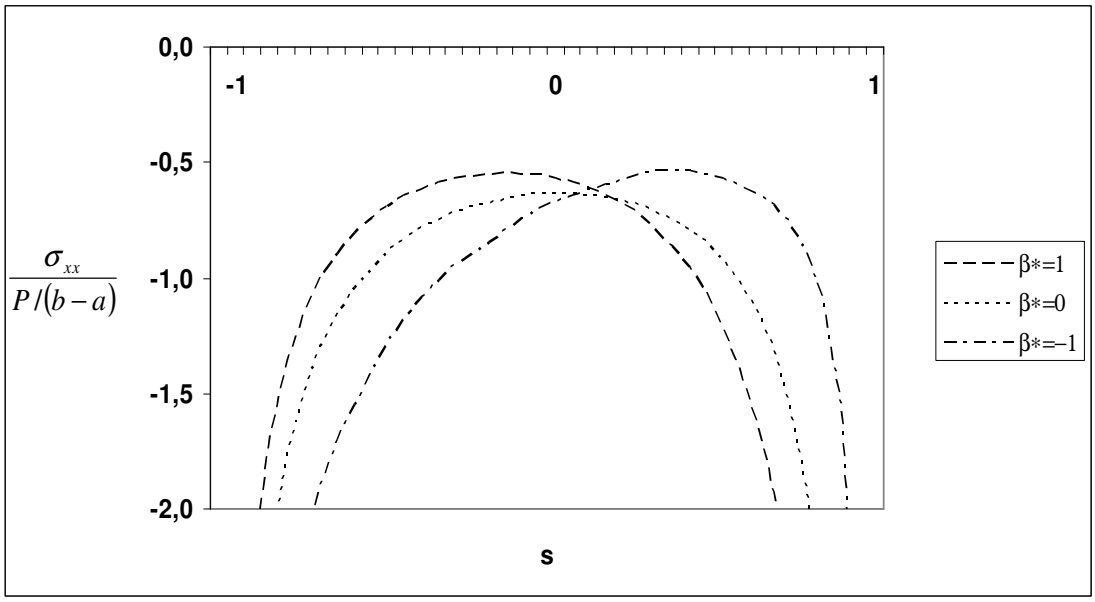

Figure 24: Normalized stress distribution for various values of the nonhomogeneity constant $\beta\,(b\text{-}a) = \beta^*$ [η = -0.6, $\gamma\,(b\text{-}a) = \gamma^*$ = -0.5 and $\gamma\,(b+a) = \gamma^{**} = \beta\,(b+a) = \beta^{**}$ =0]

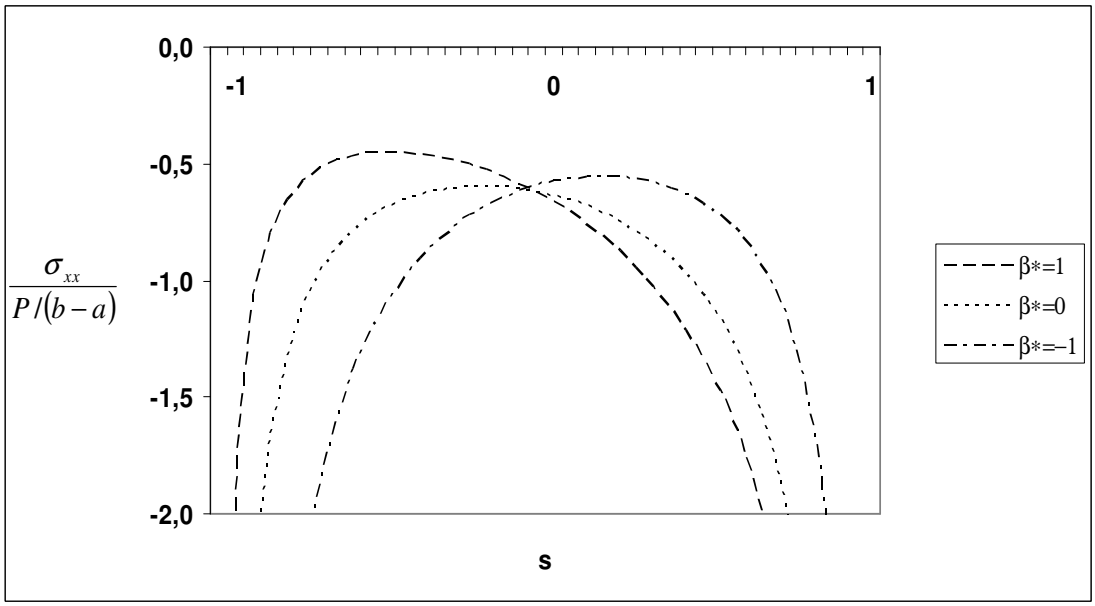

Figure 25: Normalized stress distribution for various values of the nonhomogeneity constant $\beta\,(b\text{-}a) = \beta^*$ [η = 0, $\gamma\,(b\text{-}a) = \gamma^*$ = 0.5 and $\gamma\,(b+a) = \gamma^{**} = \beta\,(b+a) = \beta^{**}$ =0]

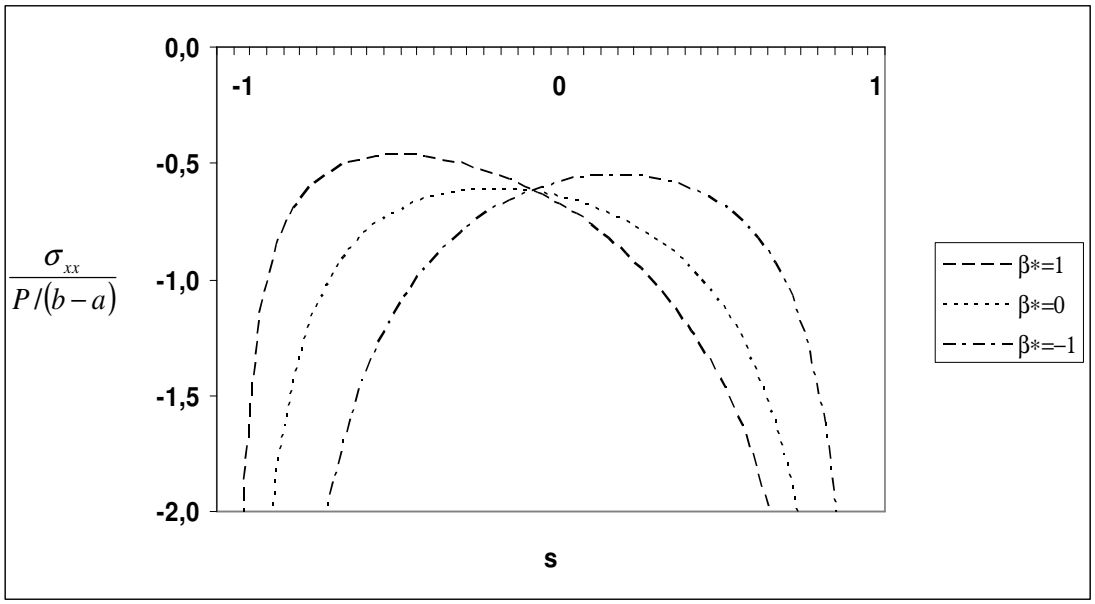

Figure 26: Normalized stress distribution for various values of the nonhomogeneity constant $\beta\,(b\text{-}a) = \beta^*$ [η = 0.2, $\gamma\,(b\text{-}a) = \gamma^* = 0.5$ and $\gamma\,(b\text{+}a) = \gamma^{**} = \beta\,(b\text{+}a) = \beta^{**} = 0$]

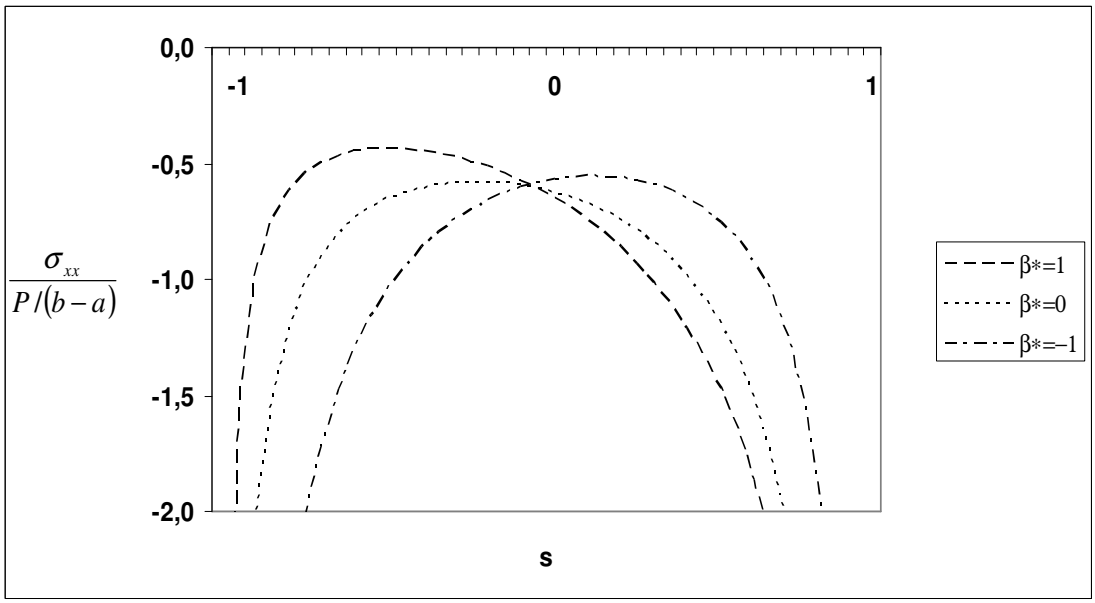

Figure 27: Normalized stress distribution for various values of the nonhomogeneity constant $\beta\,(b\text{-}a) = \beta^*$ [η = -0.2, $\gamma\,(b\text{-}a) = \gamma^* = 0.5$ and $\gamma\,(b\text{+}a) = \gamma^{**} = \beta\,(b\text{+}a) = \beta^{**} = 0$]

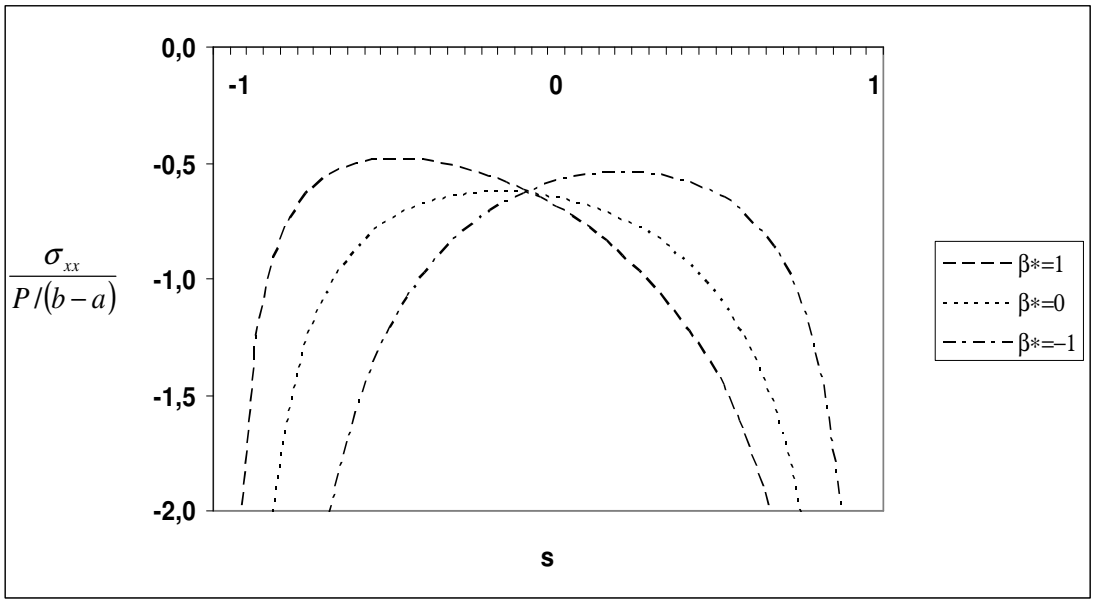

Figure 28: Normalized stress distribution for various values of the nonhomogeneity constant $\beta\,(b\text{-}a) = \beta^*$ [η = 0.4, $\gamma\,(b\text{-}a) = \gamma^* = 0.5$ and $\gamma\,(b\text{+}a) = \gamma^{**} = \beta\,(b\text{+}a) = \beta^{**} = 0$]

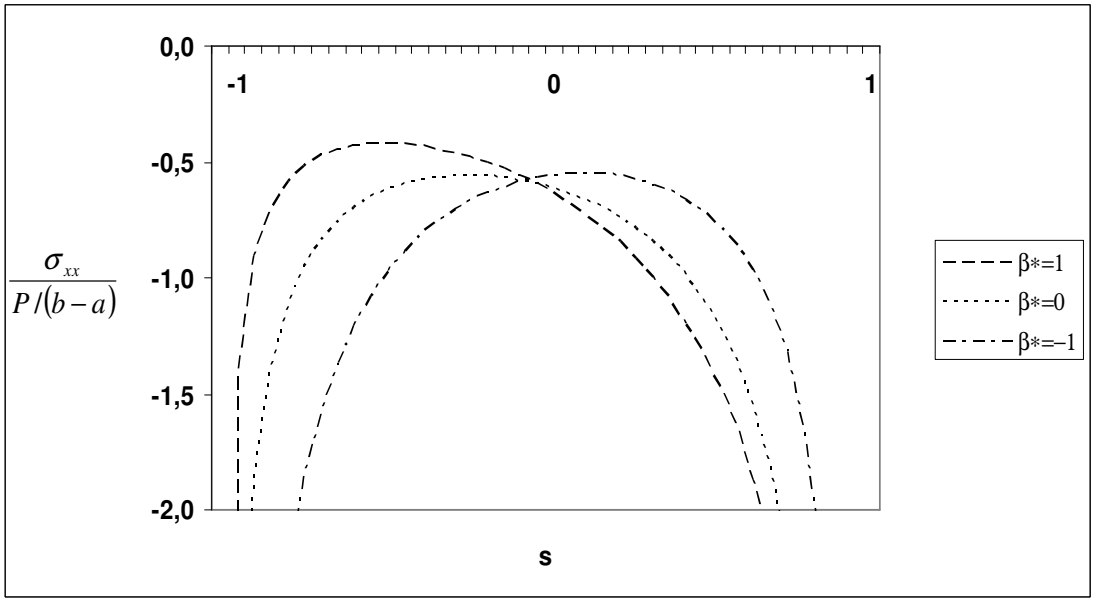

Figure 29: Normalized stress distribution for various values of the nonhomogeneity constant $\beta\,(b\text{-}a) = \beta^*$ [η = -0.4, $\gamma\,(b\text{-}a) = \gamma^* = 0.5$ and $\gamma\,(b\text{+}a) = \gamma^{**} = \beta\,(b\text{+}a) = \beta^{**} = 0$]

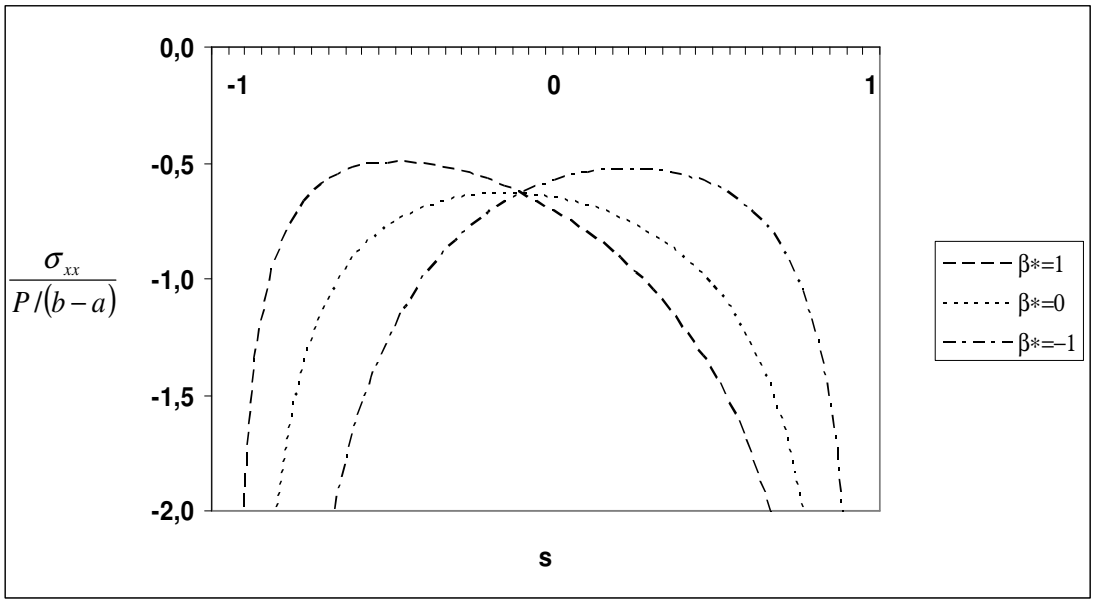

Figure 30: Normalized stress distribution for various values of the nonhomogeneity constant $\beta(b-a) = \beta^*$ [$\eta = 0.6$, $\gamma(b-a) = \gamma^* = 0.5$ and $\gamma(b+a) = \gamma^{**} = \beta(b+a) = \beta^{**} = 0$]

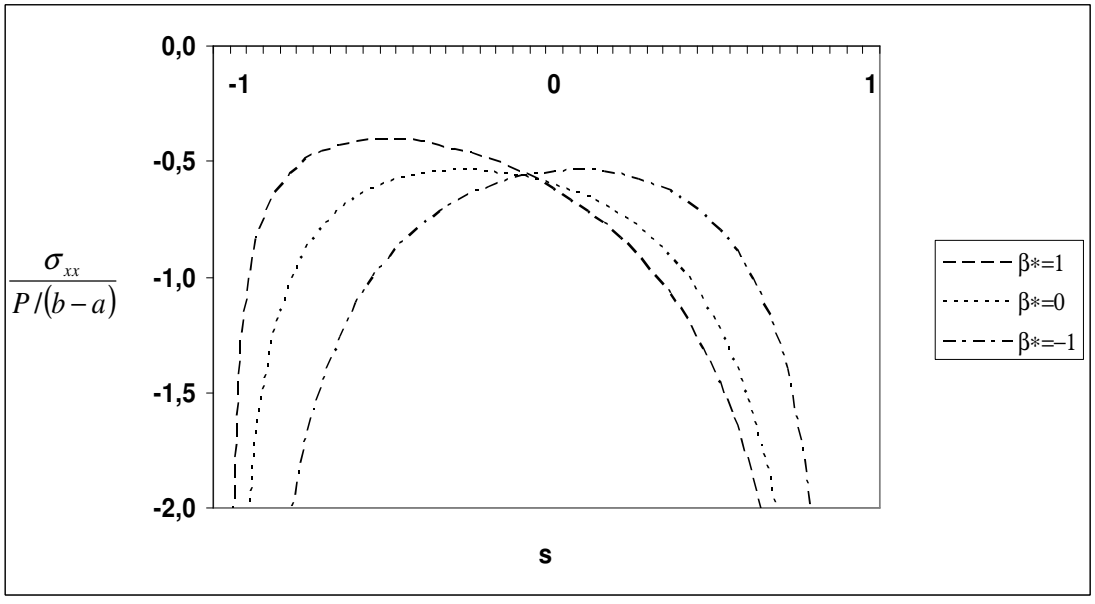

Figure 31: Normalized stress distribution for various values of the nonhomogeneity constant $\beta(b-a) = \beta^*$ [$\eta = -0.6$, $\gamma(b-a) = \gamma^* = 0.5$ and $\gamma(b+a) = \gamma^{**} = \beta(b+a) = \beta^{**} = 0$]

4.2.1 Comments on the Results Obtained for the Flat Stamp

The results is given in this section can be categorized into four groups according to the different values of nonhomogenity parameters. In each group the stress distribution is stated for the different values of the friction coefficient, namely, $\eta = 0$, $\eta = 0.2$, $\eta = -0.2$, $\eta = 0.4$, $\eta = -0.4$, $\eta = 0.6$ and $\eta = -0.6$. The negative value of friction coefficient indicates the reverse direction of the applied tangential force. As shown in the figure 2, the positive friction coefficient indicates the tangential force acting in the positive direction of *y* axis on the stamp. The zero friction coefficients are for the frictionless contact surface.

The graphs given in figures 4 - 10 are drawn when $\beta^* = \gamma^{**} = \beta^{**} = 0$, $\gamma^* = -1,0,1$ for the different values of the friction coefficient. The figure 4 shows the normalized stress distribution versus the normalized position parameter *s* for $\eta = 0$. As easily seen from the figure, for $\gamma^* = 0$ the stress distribution is symmetric. This symmetric distribution can also be observed in other graphs for $\gamma^* = 0$ for the different values of the friction coefficients. The curves are asymmetric about *s*=0 for the $\gamma^* = -1$ and $\gamma^* = 1$. The shear modulus variation is the most important factor that effects the contact stress distribution. As can be seen from figures the contact stress distribution takes the behavior of the shear modulus variation at *x*=0. In all cases the contact stress distribution takes the shape of the exponential function with a positive exponent that can be seen in $\gamma^* = 1$ curves. In $\gamma^* = -1$ curves the contact stress distribution takes the shape of the exponential function with a negative exponent. As for the positive valued friction coefficient and the negative valued friction coefficient, reversing the direction of the applied force does not significantly affect the stress distribution for $\eta = 0.2$ and for the other values of friction of coefficients. The stress distribution is increasing in the middle region of the contact area and the stress distribution is decreasing near the end points of the stamp.

The graphs between the figure 11 and figure 17 are drawn when $\beta^* = 1$, $\gamma^{**} = \beta^{**} = 0$ and $\gamma^* = -1,0,1$ for the different values of the friction coefficient. It is

seen that for $\gamma^* = 0$ the stress distribution is symmetric which is an expected result. Same behavior can also be seen in other curves for $\gamma^* = 0$ for the different values of friction coefficients. The curves are asymmetric about s=0 for the $\gamma^* = -1$ and $\gamma^* = 1$. Again as can be seen from figures the contact stress distribution takes the behavior of the shear modulus variation at x=0. In all cases the contact stress distribution takes the shape of the exponential function with a positive exponent that can be seen in $\gamma^* = 1$ curves, the contact stress distribution takes the shape of the exponential function with a negative exponent in $\gamma^* = -1$ curves as mentioned above. As easily seen from the figures, while the stress distribution is decreasing near the end points of the stamp, the stress distribution increases in the middle region of the contact area. Reversing the direction of the applied force does not affect the stress distribution for small values of friction coefficient. The contact problem has no solution for $\beta^* < 0$ [30]. Hence, no results were provided for this case.

The graphs between the figure 18 and figure 24 are drawn when γ^*=-0.5 and $\gamma^{**} = \beta^{**} = 0$, $\beta^* = -1,0,1$ and the graphs between the figure 25 and figure 31 are drawn when $\gamma^* = 0.5$ and $\gamma^{**} = \beta^{**} = 0$, $\beta^* = -1,0,1$ for the different values of the friction coefficient. The similar trends can also be observed in these figures and cases as compared with the graphs between the figure 4 and the figure 10.

As mentioned in chapter 1, while Özatağ [33] examined the effects of material nonhomogeneity and friction on contact stresses and singularities at end of the contact region for materials with lateral nonhomogeneity, Dağ and Erdoğan [32] examined the initiation and subcritical growth of surface cracks in FGMs. The behavior of graphs obtained by this study has to be compared with these studies one by one. The results obtained by this study are in very good agreement with these studies.

4.3 Concluding Remarks

1. The results obtained by computer program are very close to the results obtained by using the closed form solutions.
2. The shear modulus variation is the most important factor that affects the contact stress distribution. As can be seen from graphs the contact stress distribution takes the behavior of the shear modulus variation at x=0.
3. Generally while the stress distributions are decreasing near the end points of the contact area, the stress distributions increase in the middle region of the contact area.
4. Generally reversing the direction of the applied force does not significantly affect the stress distribution.
5. The contact problem has no solution for $\beta^*<0$ [30]. Hence, no results were provided for this case.
6. In this problem normalized contact stress depends on the effects of the material nonhomogeneity parameters $\gamma \& \beta$, coefficient of friction η, stamp size and stamp location on the contact area and constant Poisson's ratio v.
7. To use the elastically graded materials with a material nonhomogeneity both in lateral direction and thickness direction could be very suitable especially for tribological applications.

4.4 Future Work

The contact mechanics problem in this study is developed for elastically graded materials both in lateral direction and thickness direction in order to examine the effects of nonhomogenity parameters, friction of coefficient, stamp size and location on the contact area for flat stamp medium only. For more detailed results and in order to see the resistance of the graded materials in both lateral and thickness direction, the contact problem can be solved for triangular and circular stamp. At the same time an experimental study can be done to examine the physical behavior of FGM for designers.

The contact mechanics problem in this study is solved for isotropic medium. However this problem can be solved also for orthotropic medium. Because in certain applications, FGMs can have orthotropic behavior.

The model used in this study can also be studied for subsurface stresses in the semi-infinite medium. When this is done, asymptotic analyses have to be made for all stress components. In this study it is seen that while the stress distributions are decreasing near the end points of the contact area, the stress distributions increase in the middle region of the contact area. This problem can also be solved for cracking due to sliding contact for nonhomogeneous materials graded in both lateral and thickness direction.

Since nonhomogeneous materials are vital for the future in order to improve the material qualities for severe conditions, the future work mentioned above is required to understand the contact mechanics problems for nonhomogeneous materials.

REFERENCES

[1] T.L. Becker Jr., R.M. Cannon and R.O. Ritchie, 2000, “Finite crack kinking and T-stresses in functionally graded materials”, *International Journal of Solids and Structures,* Vol. 38, pp. 5545-5563.

[2] Datakis, A.P. and Vogan, J.W., 1985, "Rocket thrust chamber thermal barrier coatings", NASA Contractor Report 1750222.

[3] Houck, D.L. (editor), 1987, "Thermal Spray: Advances in Coating Technology", Proceedings of the National Thermal Spray Conference, Orlando, Florida, ASM International.

[4] DeMasi-Marcin, J.T. and Gupta, D.K., 1994, "Protective coatings in the gas turbine engine", *Surface Coating Technology*, 68/69.

[5] Drindley, W.J. (Compiler), 1995, Proceedings of the thermal barrier coating workshop, NASA-Lewis, Cleveland, Ohio.

[6] Erdogan, F., 1995, "Fracture mechanics of functionally graded materials", *Composites Engineering*, Vol. 5, No 7., pp. 753-770.

[7] Suresh, S. and Mortensen, A., 1998, *Fundamentals of Functionally Graded Materials: Processing and Thermomechanical Behavior of Graded Metals and Metal – Ceramic Composites*, IOM Communications, London, UK.

[8] Niino, M. and Maeda, S., 1990, “Recent Development Status of Functionally Gradient Materials,” *ISIJ International*, Vol. 30, pp. 699 – 703.

[9] Lee, W.Y., Stinton, D.P., Berndt, C.C., Erdogan, F., Lee, Y.D., and Mutasim, Z., 1996, “Concept of Functionally Graded Materials for Advanced Thermal Barrier Coating Applications,” *Journal of the American Ceramic Society*, Vol. 79, pp. 3003 – 3012.

[10] Xing, A., Jun, Z., Chuanzhen, H., and Jianhua, Z., 1998, "Development of an Advanced Ceramic Tool Material – Functionally Gradient Cutting Ceramics," *Materials Science and Engineering*, Vol. A248, pp. 125 – 131.

[11] Suresh, S., Olsson, M., Giannakopoulos, A.E., Padture, N.P., and Jitcharoen, J., 1999, "Engineering the Resistance to Sliding – Contact Damage Through Controlled Gradients in Elastic Properties at Contact Surfaces," *Acta Materialia*, Vol. 47, pp. 3915 – 3926.

[12] Hertz, H., 1882, "On the Contact of Elastic Solids", *J. Reine Angewanddte Mathematic*. 92, pp. 156-171.

[13] Barber, J.R. and Ciavarella, M., 2000, "Contact Mechanics", *International Journal of Solids and Structures*, Vol. 27, pp. 29 – 43.

[14] Gibson, R.E.,1967, "Some Results Concerning Displacements and Stresses in a Nonhomogeneous Elastic Half – Plane", *Geotechnique*, Vol. 17, pp.58-67.

[15] Calladine, C.R. and Greenwood, J.A., 1978, "Line and Point Loads on a Nonhomogeneous Incompressible Elastic Half – Space", *Quarterly Journal of Mechanics and Applied Mathematics*, Vol. 31, pp. 507 – 529.

[16] Brown, P.T. and Gibson, R.E., 1972, "Surface Settlement of a Deep Elastic Stratum whose Modulus Increases Linearly with Depth", *Canadian Geotechnical Journal*, Vol.9, pp. 467 – 476.

[17] Awojobi, A.O. and Gibson, R.E., 1973, "Plane Strain and Axially Symmetric Problems of a Linearly Homogeneous Elastic Half – Space", *Quarterly Journal of Mechanics and Applied Mathematics*, Vol. 26, pp. 285 – 302.

[18] Gibson, R.E. and Sills, G.C., 1975, "Settlement of a Strip on a Non-Homogeneous Orthotropic Incompressible Elastic Half – Space", *Quarterly Journal of Mechanics and Applied Mathematics*, Vol. 28, pp. 233 – 243.

[19] Kassir, M.K "Boussinesq Problems for Nonhomogeneous Solids", *ASCE Journal of Engineering Mechanics*, Vol. 98, pp. 457 – 471.

[20] Bakırtaş, I., 1980, "The Problem of a Rigid Punch on a Non – Homogeneous Elastic Half – Space", *International Journal of Engineering Science*, Vol. 18, pp. 597 – 610.

[21] Fabrikant, V.I. and Sankar, T.S., 1984, "On Contact Problems in an Inhomogeneous Half – Space", *International Journal of Solids and Structures*, Vol. 20, pp. 159 – 166.

[22] Selvadurai, A.P.S. and Lan, Q., 1998, "Axisymmetric Mixed Boundary Value Problems for an Elastic Halfspace with a Periodic Nonhomogeneity", *International Journal of Solids and Structures*, Vol. 35, pp. 1813 – 1826.

[23] Selvadurai, A.P.S., 1996, "The Settlement of a Rigid Circular Foundation Resting on a Half – Space Exhibiting a Near Surface Elastic Non-Homogeneity", *International Journal for Numerical and Analytical Methods in Geomechanics*, Vol. 20, pp. 351 – 364.

[24] Selvadurai, A.P.S., Singh, B.M. and Vrbik, J., 1986, "A Reissner – Sagoci Problem for a Nonhomogeneous Solid", *Journal of Elasticity*, Vol. 16, pp. 383 – 391.

[25] Suresh, S. and Mortensen, A., 1998, "Fundamentals of Functionally Graded Materials: Processing and Thermomechanical Behavior of Graded Metals and Metal – Ceramic Composites", IOM Communications, London, UK.

[26] Suresh, S., Olsson, M., Giannakopoulos, A.E., Padture, N.P. and Jitcharoen, J., 1999, "Engineering the Resistance to Sliding Contact Damage Through Controlled Gradients in Elastic Properties at Contact Surfaces", *Acta Materialia*, Vol. 47, pp. 3915 – 3926.

[27] Giannakopoulos, A.E. and Suresh, S., 1997, "Indentation of Solids with Gradients in Elastic Properties: Part II. Axisymmetric Indetors", *International Journal of Solids and Structures*, Vol. 34, pp. 2393 – 2428.

[28] Giannakopoulos, A.E. and Pallot, P., 2000, "Two – Dimensional Contact Analysis of Elastic Graded Materials", *Journal of the Mechanics and Physics of Solids*, Vol. 48, pp. 1597 – 1631.

[29] Güler, M.A., 2000, Contact Mechanics of FGM Coatings, Ph.D. Dissertation, Lehigh University, Bethlehem, Pennsylvania, USA.

[30] Dağ, S., 2001, Crack and Contact Problems in Graded Materials, Ph.D. Dissertation, Lehigh University, Bethlehem, Pennsylvania, USA.

[31] Dağ, S. and Erdoğan, F., 2002, "A Surface Crack in a Graded Medium Loaded by a Sliding Rigid Stamp", *Engineering Fracture Mechanics*, Vol. 69, pp. 1729 – 1751.

[32] Erdoğan, F. and Dağ, S., 2001, Cracking of a Graded Half – Plane due to Sliding Contact, Project Report, US Air Force Office of Scientific Research, Grant F49620-98-1-0028.

[33] Özatağ, C.A., 2003, Contact Mechanics of a Graded Surface with Elastic Gradation in Lateral Direction, Master of Science Thesis, The Middle East Technical University, Ankara, Turkey.

[34] Erdoğan, F., 1978, "Mixed Boundary Value Problems in Mechanics", *Mechanics Today*, Vol. 4, Nemat – Nasser, S., ed., Pergamon Press, New York, USA, pp. 1-84

APPENDIX

SOME USEFUL INTEGRALS

In this part of study the integrals involving the asymptotic expansions of the integrands of kernels that are in used computer program are given. The integrals are in the following form;

$$C_n = \int_a^{\infty} \frac{1}{\rho^n} \cos(\rho u) d\rho \tag{A1}$$

$$S_n = \int_a^{\infty} \frac{1}{\rho^n} \sin(\rho u) d\rho \tag{A2}$$

For n=1, following results are obtained using MAPLE,

$$C_i = -C_i(A|u|) \tag{A3}$$

$$S_i = sign(u)\left\{\frac{\pi}{2} - S_i(A|u|)\right\} \tag{A4}$$

where $C_i(\ )$ and $S_i(\ )$ are cosine and sine integrals, they are defined as

$$C_i(x) = \gamma_0 + \ln(x) + \int_0^x \frac{\cos(\alpha) - 1}{\alpha} d\alpha \tag{A5}$$

$$S_i(x) = \int_0^x \frac{\sin(\alpha)}{\alpha} d\alpha \tag{A6}$$

γ_0 is the Euler constant which is equal to 0.5772156649. For n>1, integrating the equations (A1) and (A2) by parts, the following general recursive relations can be obtained,

$$C_n = -\frac{1}{1-n}\frac{\cos(uA)}{A^{n-1}} + \frac{u}{1-n}S_{n-1}, n > 1 \tag{A7}$$

$$S_n = -\frac{1}{1-n}\frac{\sin(uA)}{A^{n-1}} - \frac{u}{1-n}C_{n-1}, n > 1 \tag{A8}$$